

# A finite-element discretization of some boundary value problems for nonlinear strain-limiting elastic bodies

Mathematics and Mechanics of Solids

2022, Vol. 27(2) 281–307

© The Author(s) 2021

Article reuse guidelines:

sagepub.com/journals-permissions

DOI: 10.1177/10812865211020789

journals.sagepub.com/home/mms



**Hyun C. Yoon**

*Department of Mathematics and Statistics, Texas A&M University-Corpus Christi, Corpus Christi, TX, USA  
Petroleum & Marine Division, Korea Institute of Geoscience and Mineral Resources, Daejeon, Republic of Korea*

**S. M. Mallikarjunaiah** 

*Department of Mathematics and Statistics, Texas A&M University-Corpus Christi, Corpus Christi, TX, USA*

Received 21 July 2020; accepted 9 May 2021

## Abstract

It is well known that the linearized theory of elasticity admits the logically inconsistent solution of singular strains when applied to certain naive models of fracture while the theory is a first-order approximation to finite elasticity in the asymptotic limit of infinitesimal displacement gradient. Meanwhile, the strain-limiting models, a special subclass of nonlinear implicit constitutive relations, predict uniformly bounded strain in the whole material body including at the strain-concentrator such as a crack tip or reentrant corner. Such a nonlinear approximation cannot be possible within the standard linearization procedure of either Cauchy or Green elasticity. In this work, we examine a finite-element discretization for several boundary value problems to study the state of stress-strain in the solid body of which response is described by a nonlinear strain-limiting theory of elasticity. The problems of notches, oriented cracks, and an interface crack in anti-plane shear are analyzed. The numerical results indicate that the linearized strain remains below a value that can be fixed *a priori*, therefore, ensuring the validity of the nonlinear model. In addition, we find high stress values in the neighborhood of the crack tip in every example, thereby suggesting that the crack tip acts as a singular energy sink for a stationary crack. We also calculate the stress intensity factor (SIF) in this study. The computed value of SIF in the nonlinear strain-limiting model is corresponding to that of the classical linear model, and thereby providing a tenet for a possible local criterion for fracture. The framework of strain-limiting theories, within which the linearized strain bears a nonlinear relationship with the stress, can provide a rational basis for developing physically meaningful models to study a crack evolution in elastic solids.

## Keywords

Strain-limiting model, V-notch, crack, anti-plane shear, nonlinear elasticity, finite-element method

---

## Corresponding author:

S. M. Mallikarjunaiah, Department of Mathematics & Statistics, Texas A&M University-Corpus Christi, 6300 Ocean Drive, Corpus Christi, TX 78412-5825, USA.

Email: m.muddamallappa@tamuucc.edu

## I. Introduction

The strategy for structural design to avoid “damage” has been an important approach in the area of engineering and material design from recent decades. One of the well-known examples of damage-based design would be the aircraft engine turbine blade. Designing such damage-resistant structures is indisputably very important, because of the huge cost of safety and economics involved. This is more like “prevention is better than cure” principle with its main objective being to impede the fracture-based damage or failure of material structures. Brittle or fatigue cracks, at the micro or macro level, are inherently dangerous to the structures due to the sudden impact and permanent failure of engineering architecture that carry high loads. Thus, prior and exact knowledge of stress-strain distribution in such structures is very important for the safe design practice.

The computation of stress-strain in the neighborhood of pre-existing defects such as notches, slits, holes, or damage inclusions is an important problem in both industry and academia. The issue has been primarily studied within the context of constitutive relations of linearized theory of elasticity [1–4]. One of the major areas discontent about the classical elasticity model is that, being a first-order linear approximation of finite elasticity, it predicts the unphysical near-tip strain singularity. Several studies [5–10] have been carried out to augment the classical model for achieving physically meaningful constitutive relations that can correctly predict the real phenomenon. However, many such augmentations are either computationally cumbersome or difficult to validate experimentally [11].

Furthermore, within the context of linear elastic fracture mechanics (LEFM), modeling crack initiation and its evolution has some significant issues that need to be handled properly. In addition to the development of strain singularity at the crack tip, they include a blunt shaped crack-opening profile, and the possibility of inter-penetration of crack faces when the theory is applied to model the crack at a bimaterial interface. Specifically, the aforementioned strain singularity cannot be avoided even when one thrusts the problem within the nonlinear elasticity as done by Knowles and Sternberg in their seminal paper [12] or with the bell constraint model by Tarantino in [13]. Thus, a very important question can be posed whether or not the algebraic nonlinear models manage to regulate the crack-tip strain singularity even if the stresses are large.

A generalization of Cauchy and Green elasticity has been initiated by Rajagopal and his co-authors in a series of papers [14–22], in which the authors describe the implicit constitutive models that have a strong tenor of thermodynamic framework. The response of an elastic body<sup>1</sup> is best described by the implicit constitutive relations between Cauchy stress and deformation gradient tensors [23–26]. A crucial feature of Rajagopal’s proposal is a prospect of obtaining a special hierarchy of “explicit” nonlinear relationship for the linearized strain as a nonlinear function of Cauchy stress. Then, through a conspicuous subclass of implicit models, the linearized strain can be depicted with a uniformly bounded function throughout the material body, even when the stress is very large. Such a *limiting strain* property makes these models a paradigmatic choice to study behavior of cracks and fractures in brittle materials [7, 27–29], including any possibility of extending them to the study of quasi-static or even dynamic crack evolution. Using the strain-limiting models, several studies have attempted to revisit the classical problems in elasticity such as two-dimensional V-notches [30–33], elliptical holes [34–36], unsteady problems [37–41], and nonlinear viscoelastic deformations [42–45]. A rigorous mathematical analysis has been carried out in [31, 46–49] concerning the existence and uniqueness of weak solutions for the large class of strain-limiting models.

The purpose of this work is to study a finite-element discretization of some boundary value problems for nonlinear strain-limiting elastic bodies and to deliberate the stress-strain behavior within the context of nonlinear models. Three main problems in anti-plane shear are studied in this paper: V-notches up to that with zero notch angle, oriented cracks, and an interface crack. Comparing the classical linear model and the nonlinear strain-limiting model, the stress intensity factor (SIF) values are also calculated. In particular, the aim is to lay out the differences in near-tip stress-strain predictions.

## 2. Mathematical formulation

In this section, we provide definitions and a brief overview of the nonlinear strain-limiting elasticity model. We present the nonlinear constitutive framework using the kinematical variables and notations of classical linearized elasticity.

## 2.1. Kinematics and basic equations of classical elasticity

Let  $\mathcal{A}$  be an abstract material body occupying a region in  $\mathbb{R}^d$ ,  $d \in \{2, 3\}$ , and the boundary of  $\mathcal{A}$  be assumed to be Lipschitz. Let  $\kappa_R(\mathcal{A})$  and  $\kappa_t(\mathcal{A})$  denote the reference and deformed configurations of the material body,  $\mathcal{A}$ , respectively. Let  $\mathbf{x} := f(\mathbf{X}, t)$  denote the current position of a particle (motion of a particle) that is at  $\mathbf{X}$  in a stress-free reference configuration of the material body, where the variable  $t$  denotes the time. Here,  $f$  is a deformation of the body which is assumed to be “smooth” and the displacement is denoted by  $\mathbf{u} := \mathbf{x} - \mathbf{X}$ . The displacement gradients are defined

$$\frac{\partial \mathbf{u}}{\partial \mathbf{X}} := \nabla_{\mathbf{X}} \mathbf{u} = \mathbf{F} - \mathbf{I} \quad \text{and} \quad \frac{\partial \mathbf{u}}{\partial \mathbf{x}} := \nabla_{\mathbf{x}} \mathbf{u} = \mathbf{I} - \mathbf{F}^{-1}, \quad (1)$$

where  $\mathbf{I}$  is the second-order identity tensor and  $\mathbf{F}$  is the deformation gradient

$$\mathbf{F} := \frac{\partial f}{\partial \mathbf{X}}. \quad (2)$$

The left and right Cauchy–Green stretch tensors  $\mathbf{B}$  and  $\mathbf{C}$  are given by

$$(\text{left}) \quad \mathbf{B} := \mathbf{FF}^T, \quad (\text{right}) \quad \mathbf{C} := \mathbf{F}^T \mathbf{F}, \quad (3)$$

respectively. Then, the Green–St. Venant strain tensor  $\mathbf{E}$  and the Almansi–Hamel strain  $\mathbf{e}$  are defined

$$\mathbf{E} := \frac{1}{2}(\mathbf{C} - \mathbf{I}) \quad \text{and} \quad \mathbf{e} := \frac{1}{2}(\mathbf{I} - \mathbf{B}^{-1}). \quad (4)$$

Let  $\boldsymbol{\sigma}$  denote the Cauchy stress tensor in the deformed configuration, then the first and second Piola–Kirchhoff stress tensors, denoted as  $\mathbf{S}$  and  $\tilde{\mathbf{S}}$ , respectively in the reference configuration, are defined by

$$\mathbf{S} := \boldsymbol{\sigma} \mathbf{F}^{-T} \det(\mathbf{F}) \quad \text{and} \quad \tilde{\mathbf{S}} := \mathbf{F}^{-1} \mathbf{S}. \quad (5)$$

The body  $\mathcal{A}$  is said to be *Green elastic* (or *hyperelastic*) [50] if the stress response is the function of gradient of a scalar-valued potential, i.e.,

$$\hat{\mathbf{S}}(\mathbf{F}) = \partial_{\mathbf{F}} \hat{w}(\mathbf{F}), \quad (6)$$

if a stored energy exists for the material body under consideration. The body is said to be *Cauchy elastic* if its constitutive class of the relationship is determined by a scalar response function of the form as

$$\mathbf{S} = \tilde{\mathbf{S}}(\mathbf{F}). \quad (7)$$

In the theory of linearized elasticity, the assumption that the displacement gradients are “infinitesimal” is taken to be

$$\max \| \nabla_{\mathbf{x}} \mathbf{u} \| = \mathcal{O}(\delta), \quad \delta \ll 1, \quad (8)$$

where  $\| \cdot \|$  is the *Frobenius norm*. Using (8), it follows that:

$$\mathbf{E} = \mathbf{e} + \mathcal{O}(\delta^2), \quad \mathbf{e} = \mathbf{e} + \mathcal{O}(\delta^2), \quad \mathbf{B} = \mathbf{I} + 2\mathbf{e} + \mathcal{O}(\delta^2), \quad (9)$$

where  $\mathcal{O}$  is *big-O*-notation and  $\mathbf{e}$  is the customary linearized (or engineering) strain tensor defined as

$$\mathbf{e} := \mathbf{e}(\mathbf{u}) = \frac{1}{2} (\nabla \mathbf{u} + (\nabla \mathbf{u})^T), \quad (10)$$

where  $(\cdot)^T$  is the *transpose* operator applied to the second-order tensor. The meaningful strain measure under the assumption (8) is the linearized strain (10). Therefore, there is no distinction between the variables in current and reference configurations.

The balance of linear and angular momentum are given by the equations

$$\rho \frac{d\mathbf{v}}{dt} = \operatorname{div}(\boldsymbol{\sigma}) + \mathbf{b}, \quad (11)$$

and

$$\boldsymbol{\sigma} = \boldsymbol{\sigma}^T, \quad (12)$$

where in (11)  $\rho$  is the density of the material in current configuration,  $\mathbf{v}$  is the velocity, and  $\mathbf{b}$  is the body force term. For the quasi-static problem, in the absence of body force, the equilibrium equation reduces to

$$\operatorname{div}(\boldsymbol{\sigma}) = \mathbf{0}. \quad (13)$$

For a given strain field  $\boldsymbol{\epsilon}$  in the domain  $\kappa_R(\mathcal{A})$ , along with the balance of linear momentum (13), the compatibility condition guarantees the existence of unique, smooth displacement field  $\mathbf{u}$ . It is given by

$$\operatorname{curl} \operatorname{curl} \boldsymbol{\epsilon} = \mathbf{0}, \quad (14)$$

where “curl” is the classical *curl* operator defined in the space of second-order tensors. For the classical isotropic, homogeneous, linear elastic material, the constitutive relationship, between stress and strain, is given by

$$\boldsymbol{\sigma} := 2\mu \boldsymbol{\epsilon} + \lambda \operatorname{tr}(\boldsymbol{\epsilon}) \mathbf{I}, \quad (15)$$

where  $\mu$  and  $\lambda$  are Lamé parameters and “ $\operatorname{tr}(\cdot)$ ” is the trace operator for tensors. It is worth noting that (15) is invertible and one can express the linearized strain tensor as a (linear) function of Cauchy stress

$$\boldsymbol{\epsilon} = \frac{1}{2\mu} \boldsymbol{\sigma} - \frac{\lambda}{2\mu(\lambda + \frac{2}{d}\mu)d} \operatorname{tr}(\boldsymbol{\sigma}) \mathbf{I}, \quad (16)$$

where  $d$  is the dimension number. The relation (16) between the linearized strain and the stress is yet linear and can also model the response of materials within the framework of linear elasticity. Equation (16) is well defined because both  $\mu > 0$  and  $(\lambda + \frac{2\mu}{d}) > 0$ .

## 2.2. Nonlinear implicit and strain-limiting constitutive models

Recently, Rajagopal and coauthors [14–17, 19] showed that the class of elastic bodies is far richer and more general than the class of elastic bodies described as Cauchy and Green elasticity. Rajagopal’s generalization [15] assumes that Cauchy stress  $\boldsymbol{\sigma}$  and Cauchy–Green stretch  $\mathbf{B}$  are related implicitly by a relation of the form:

$$\mathcal{F}(\boldsymbol{\sigma}, \mathbf{B}) = \mathbf{0}, \quad (17)$$

where  $\mathcal{F}$  is assumed to be an isotropic function which satisfy the relation:

$$\mathcal{F}(Q\boldsymbol{\sigma}Q^T, Q\mathbf{B}Q^T) = Q\mathcal{F}(\boldsymbol{\sigma}, \mathbf{B})Q^T, \quad \forall Q \in O, \quad (18)$$

where  $O$  denotes the distance-preserving orthogonal group. A special subclass of these implicit models is an explicit representation which is given for the left Cauchy–Green stretch tensor  $\mathbf{B}$  in terms of Cauchy stress  $\boldsymbol{\sigma}$

$$\mathbf{B} = \mathcal{F}(\boldsymbol{\sigma}). \quad (19)$$

For these models (19), if there exists a constant  $M > 0$  such that

$$\sup_{\boldsymbol{\sigma} \in \operatorname{Sym}} |\mathcal{F}(\boldsymbol{\sigma})| \leq M, \quad (20)$$

are known as the *strain-limiting constitutive relations*. Here  $\operatorname{Sym}$  denotes the vector space of symmetric, second-order tensors over  $\mathbb{R}^3$ .

For the isotropic bodies, a general explicit representation of the left Cauchy–Green stretch tensor  $\mathbf{B}$  by

$$\mathbf{B} = \tilde{\alpha}_1 \mathbf{I} + \tilde{\alpha}_2 \boldsymbol{\sigma} + \tilde{\alpha}_3 \boldsymbol{\sigma}^2, \quad (21)$$

where  $\tilde{\alpha}_i$ ,  $i = 1, 2, 3$ , are the scalar functions of the isotropic invariants of the Cauchy stress

$$\rho, \operatorname{tr}(\boldsymbol{\sigma}), \operatorname{tr}(\boldsymbol{\sigma}^2), \operatorname{tr}(\boldsymbol{\sigma}^3).$$

Finally, the linearization of the model (21) under the assumption of small displacement gradient as (8)–(9) leads to

$$\mathbf{I} + 2\boldsymbol{\epsilon} + \mathcal{O}(\delta^2) = \tilde{\alpha}_1 \mathbf{I} + \tilde{\alpha}_2 \boldsymbol{\sigma} + \tilde{\alpha}_3 \boldsymbol{\sigma}^2, \quad (22)$$

$$\boldsymbol{\epsilon} = \beta_1 \mathbf{I} + \beta_2 \boldsymbol{\sigma} + \beta_3 \boldsymbol{\sigma}^2, \quad (23)$$

where the linearized strain  $\boldsymbol{\epsilon}$  is given as a nonlinear function of Cauchy stress  $\boldsymbol{\sigma}$  and here the material moduli  $\beta_i$ ,  $i = 1, 2, 3$ , depend upon the principal invariants of  $\boldsymbol{\sigma}$ . It is important to know that the relation (23) has subtle importance in studying problems involving cracks and fractures. In (23),  $\boldsymbol{\epsilon}$  is required to be “small” whereas there is no such restriction on the stress  $\boldsymbol{\sigma}$ . Even though the stress can be arbitrarily large, but one can limit strains by choosing the upper-bound value *a priori*.

Now, let us consider the special subclass of strain-limiting constitutive relationship (23) of the form,

$$\boldsymbol{\epsilon} = \Psi_0(\text{tr}(\boldsymbol{\sigma})) \mathbf{I} + \Psi_1(\|\boldsymbol{\sigma}\|) \boldsymbol{\sigma}, \quad (24)$$

and which is generally non-invertible. In (24), the functions  $\Psi_0: \mathbb{R} \rightarrow \mathbb{R}$  and  $\Psi_1: \mathbb{R}_+ \rightarrow \mathbb{R}$  are scalar functions of the invariants of the Cauchy stress and, more importantly, the assumption of no residual strain implies  $\Psi_0(x) = 0$ . Moreover, both functions  $\Psi_0$  and  $\Psi_1$  are assumed to be continuous and almost everywhere differentiable functions. In (24), the operator  $\|\cdot\|$  is the *Frobenius norm* of second-order tensor. For any two second-order tensors  $\mathbf{S}$  and  $\mathbf{T}$ , the *colon* operator is defined as

$$\mathbf{S}: \mathbf{T} = \sum_{i=1}^d \sum_{j=1}^d (\mathbf{S})_{ij} (\mathbf{T})_{ij}, \quad (25)$$

then the *Frobenius norm* is defined as

$$\|\mathbf{S}\| := \sqrt{\mathbf{S}: \mathbf{S}}. \quad (26)$$

### 3. Anti-plane shear problem

In this work, our aim is to portray the difference in stress–strain predictions by the nonlinear model and the classical linearized model. To that end, we study the state of anti-plane shear problem within the context of strain-limiting theory of elasticity. The anti-plane shear is planar, meaning that quantities such as displacement vector  $\mathbf{u}(x)$ , stress tensor  $\boldsymbol{\sigma}(x)$ , and strain tensor  $\boldsymbol{\epsilon}(x)$  depend only upon the in-plane coordinates  $x_1$  and  $x_2$ . Thus, the in-plane displacements are zero, while the out-of-plane displacement is dependent on in-plane variables  $x_1$  and  $x_2$  but independent of  $x_3$ . Therefore, the only non-zero component of the displacement vector is in  $x_3$ -direction, i.e.,

$$\mathbf{u}(x_1, x_2) = (0, 0, u(x_1, x_2)). \quad (27)$$

Further, the only non-zero components of the stress tensor  $\boldsymbol{\sigma}$  are  $\sigma_{13}$  and  $\sigma_{23}$  and the corresponding non-zero strain components are  $\epsilon_{13}$  and  $\epsilon_{23}$ . Then, the constitutive relationship for linear materials reduces to

$$\boldsymbol{\sigma} = 2\mu \boldsymbol{\epsilon}, \quad (28)$$

where  $\mu$  is the reference shear modulus. For the planar problem on hand, with only two non-zero strain components  $\epsilon_{13}$  and  $\epsilon_{23}$ , (14) takes the form

$$\frac{\partial}{\partial x_2} \epsilon_{13} - \frac{\partial}{\partial x_1} \epsilon_{23} = 0. \quad (29)$$

In order to obtain a boundary value problem within the nonlinear strain-limiting theory, we introduce the scalar Airy's stress function,  $\Phi = \Phi(x_1, x_2)$ , then

$$\sigma_{13} := \frac{\partial \Phi}{\partial x_2}, \quad \sigma_{23} := -\frac{\partial \Phi}{\partial x_1}, \quad (30)$$

which automatically satisfies the equilibrium equation (13).

From (27) and (28), it is clear that  $\text{tr}(\boldsymbol{\sigma}) = 0$ , therefore (24) reduces to

$$\boldsymbol{\epsilon} = \Psi_1(\|\boldsymbol{\sigma}\|)\boldsymbol{\sigma}. \quad (31)$$

Then, using (30) in (31), we get

$$\epsilon_{13} = \Psi_1(\|\nabla\Phi\|)\Phi_{,2} \quad (32a)$$

$$\epsilon_{23} = -\Psi_1(\|\nabla\Phi\|)\Phi_{,1}, \quad (32b)$$

and now using (32) in (29), we obtain a second-order quasi-linear partial differential equation (PDE)

$$-\nabla \cdot (\Psi_1(\|\nabla\Phi\|) \nabla\Phi) = 0, \quad (33)$$

with

$$\|\nabla\Phi\|^2 = (\partial_{x_1}\Phi)^2 + (\partial_{x_2}\Phi)^2. \quad (34)$$

In the remainder of this paper, for illustrative purposes, we use the following particular form of the constitutive function  $\Psi_1(\cdot)$ ,

$$\Psi_1(\|\boldsymbol{\sigma}\|) = \frac{1}{2\mu(1 + \beta\|\boldsymbol{\sigma}\|^\alpha)^{1/\alpha}}, \quad (35)$$

where the positive constants  $\beta$  and  $\alpha$  are the modeling parameters. A similar form has been used to study stress-strain near a static wedge [30, 33] and elliptical hole [34].

An important feature of the choice of the constitutive function  $\Psi_1(\cdot)$  is the existence of uniform bound

$$\lim_{\xi \rightarrow \infty} \xi \Psi_1(\xi) = \frac{1}{2\mu\beta^{1/\alpha}},$$

which implies that the strains are uniformly bounded throughout the body and the bound can be fixed *a priori* as

$$\|\boldsymbol{\epsilon}\| \leq \frac{1}{2\mu\beta^{1/\alpha}}.$$

It is also important to note that, if the parameter  $\beta$  tends to zero in (35), then the nonlinear strain-limiting model (32) reduces to the classical linearized elasticity model.

**Remark 3.1.** *It is well reported that the linearized theory of elasticity coupled with traction-free crack-surface boundary condition predicts both strain and stress proportional to  $1/\sqrt{r}$  where  $r$  is the radial distance to the crack-tip. However, such a result is self-contradictory with the linearization assumption under which the theory is predicated. Meanwhile, the constitutive relation (31) has no restrictions on the stress, while requiring the strain to be infinitesimal. Moreover, nonlinear constitutive relationship as (31) cannot be obtained by the same linearization procedure applied to Cauchy or Green elasticity [22].*

**Remark 3.2.** *A systematic derivation of thermodynamically consistent implicit constitutive theory was originated in [14]. The models introduced in [14] are non-dissipative and non-hyperelastic. Important questions can include whether (31) possesses an equivalent hyperelastic formulation (or Green-elasticity-like description) and more specifically, under what conditions the response function  $\Psi_1$  in (31) is invertible. It was shown in [51, 52] that for a general subclass of strain-limiting type of models, the invertibility of the response function is unique only when the strains are sufficiently small. In [53], it was shown that there is a special subclass of material models for which there exists a scalar-valued energy function  $\bar{w}(\boldsymbol{\sigma})$ , such that*

$$\boldsymbol{\epsilon} = \frac{\partial \bar{w}(\boldsymbol{\sigma})}{\partial \boldsymbol{\sigma}}. \quad (36)$$

*Further, the hyperelastic strain-limiting nonlinear models can be defined via “complementary energy” function [27] as*

$$\boldsymbol{\sigma} = \partial_{\boldsymbol{\epsilon}} \hat{h}(\|\boldsymbol{\epsilon}\|). \quad (37)$$

*For a special case with  $\alpha = 1$  in (35) and combining (31), one can readily show that*

$$\hat{h}(r) = -\frac{1}{\beta^2} (\ln(1 - \beta r) + \beta r). \quad (38)$$

In view of (35), the nonlinear PDE (33) now takes the form

$$-\nabla \cdot \left( \frac{\nabla \Phi}{2\mu(1+\beta\|\nabla\Phi\|^\alpha)^{1/\alpha}} \right) = 0. \quad (39)$$

This second-order, quasi-linear PDE, for certain values of modeling parameters  $\beta$  and  $\alpha$ , is concurrent with the classical minimal surface optimality problem from variational mechanics. In [54], for a non-convex V-notch domain and by employing dual variational methods, the authors have proved the existence of a continuous solution to the anti-plane shear problem for  $\alpha \in (0, 2)$  and  $\beta > 0$ .

**Formulation:** Given a Dirichlet boundary value,  $\mathbf{g} := (0, 0, g(x_1, x_2))$ , we seek the *Airy's stress potential*  $\Phi: \Omega \rightarrow \mathbb{R}$  such that

$$-\nabla \cdot \left( \frac{\nabla \Phi}{2\mu(1+\beta\|\nabla\Phi\|^\alpha)^{1/\alpha}} \right) = 0, \quad \text{in } \Omega, \quad (40)$$

$$\Phi = g(x_1, x_2), \quad \text{in } \partial\Omega. \quad (41)$$

The Dirichlet boundary condition (41) for the Airy potential  $\Phi$  corresponds to a pure traction boundary value problem for the corresponding physical boundary value problem. Interested readers can find the details on how to derive the boundary conditions in [30, 33]. In the current work, we seek the solution to the above formulation by using an appropriate numerical method for different boundary value problems.

## 4. Finite-element formulation

Let  $\kappa_t(\mathcal{A})$  be the closure of an open, connected, bounded domain in  $\mathbb{R}^2$ , with Lipschitz boundary  $\partial\kappa_t(\mathcal{A})$ . We assume a boundary partition such as

$$\partial\kappa_t(\mathcal{A}) = \overline{\partial\kappa_t(\mathcal{A}_D)} \cup \overline{\partial\kappa_t(\mathcal{A}_N)} \quad \text{and} \quad \partial\kappa_t(\mathcal{A}_D) \cap \partial\kappa_t(\mathcal{A}_N) = \emptyset$$

consisting of a Neumann boundary  $\partial\kappa_t(\mathcal{A}_N)$  and a non-empty Dirichlet boundary  $\partial\kappa_t(\mathcal{A}_D)$ . Let  $\Gamma_c \subset \kappa_t(\mathcal{A})$  be a geometrical boundary of a surface (e.g., notch, crack, or slit) out of the bulk volume. For example, the limit of vanishing angle between the faces of the V-notch is the crack. For readability, we introduce the following simplified notations of the form:

$$\kappa_t(\mathcal{A}) = \Omega, \quad \partial\kappa_t(\mathcal{A}) = \Gamma, \quad \partial\kappa_t(\mathcal{A}_D) = \Gamma_D, \quad \partial\kappa_t(\mathcal{A}_N) = \Gamma_N.$$

### 4.1. Function spaces

Here we use some standard notations: italic letters (e.g.,  $f$ ) denote scalar-valued functions in  $\mathbb{R}^2$ ; bold letters (such as  $\sigma, \epsilon$ ) are for the second-order, real-valued, tensors defined on the domain  $\Omega$ . The spaces of real-valued functions on  $\mathbb{R}^2$  are denoted by capital italic letters (e.g.,  $L^2(\Omega)$ ). Let  $X$  be a space of all real-valued functions defined on  $\Omega$  with an inner product defined by

$$(f, g)_X := \int_{\Omega} f g \, dx,$$

and  $L^p(\Omega, X)$  is the space of all *Lebesgue integrable functions* defined on  $\Omega$ . The norm  $\|\cdot\|_{L^p}$  is defined as

$$\|u\|_{L^p} = \left( \int_{\Omega} \|u\|_X^p \, dx \right)^{1/p}, \quad p \in [1, \infty). \quad (42)$$

The usual space of  $L^2$  is the space of square integrable functions and we denote by  $\|\cdot\|$  and  $(\cdot, \cdot)$  the norm and inner product, respectively, defined over  $L^2(\Omega, X)$  unless otherwise noted. For any  $b \in \mathbb{N}$ ,  $b \geq 0$ , we denote by  $W^{b,p}(\Omega)$  for the space of functions in  $L^p(\Omega, X)$  admitting the weak derivatives up to  $p$ th order, i.e.,

$$W^{b,p}(\Omega) := \{u \in L^p(\Omega) : D^\alpha u \in L^p(\Omega), \forall \alpha \text{ with } |\alpha| \leq b\}. \quad (43)$$

The space  $W^{b,p}(\Omega)$  is equipped with the norm

$$\|u\|_{W^{b,p}(\Omega)} := \sum_{|\alpha| \leq b} \|D^\alpha u\|_{L^p(\Omega)}. \quad (44)$$

In particular,  $H^1(\Omega) := W^{1,2}(\Omega)$  is the Hilbert space defined as

$$H^1(\Omega) := \{u \in L^2(\Omega) : Du \in L^2(\Omega)\}, \quad (45)$$

and by  $H_0^1(\Omega)$  for its subspace that takes zero boundary trace defined as

$$H_0^1(\Omega) := \{u \in H^1(\Omega) : u = 0 \text{ on } \partial\Omega\}. \quad (46)$$

The space  $W_0^{1,2}(\Omega)$  is an approximation space for *Airy's stress potential function* and  $H^{-1}(\Omega)$  is the dual space for  $H^1$ . The Sobolev norm  $\|\cdot\|_{H^1(\Omega)}$  is of the form

$$\|v\|_{H^1(\Omega)} := \left( \|v\|_{L^2(\Omega)}^2 + \|\nabla v\|_{L^2(\Omega)}^2 \right)^{1/2}, \quad (47)$$

for any function  $v \in H^1(\Omega)$ . Then  $\|\cdot\|_{H^{-1}(\Omega)}$  is the dual norm with respect to  $\|\cdot\|_{H^1(\Omega)}$ .

#### 4.2. Numerical method

Let  $\Omega \subset \mathbb{R}^2$ , and  $\Omega$  be an open, bounded, Lipschitz, connected domain with the boundary  $\partial\Omega$  consisting of two smooth disjoint parts  $\Omega_D$  and  $\Omega_N$  such that  $\partial\Omega = \overline{\Omega_D \cup \Omega_N}$ . Moreover, we assume that  $\Omega_D \neq \emptyset$ . We consider the following problem: given  $g(x) : \Omega_D \rightarrow \mathbb{R}$  is a continuous function, then find  $\Phi \in H^2(\Omega)$  such that

$$-\nabla \cdot \left( \frac{\nabla \Phi}{2\mu(1 + \beta\|\nabla \Phi\|^\alpha)^{1/\alpha}} \right) = 0, \quad \text{in } \Omega, \quad (48)$$

subjected to the boundary conditions

$$\Phi = g(x), \quad \forall x \in \Omega_D. \quad (49)$$

We adopt the same boundary conditions as in [30] for a problem with “Airy’s stress” potential function as the unknown. For a detailed discussion on the derivation of boundary conditions for  $\Phi$  starting with the traction boundary conditions, we refer the interested reader to [30].

**4.2.1. Linearization and Newton’s method.** The *quasi-linear PDE* (48) is not acquiescent to any closed-form solution methods. Therefore, we use a numerical method, based on bilinear finite elements, to find an *approximate numerical solution*. We are interested in characterizing the difference in prediction between the classical linear model and the nonlinear model proposed in this paper. To be clear, the focus of this work is to verify the nonlinear model, but not to make any promise on the optimality of the finite-element discretization used for the PDE using the standard Galerkin finite-element method. A more focused numerical work is an interesting subject within the framework of nonlinear implicit models and will be a topic for future study.

Before we formulate a discrete finite-element method for the purpose of solving the model (48)–(49), we first linearize the PDE (48) by *Newton’s method*. The superscript  $n \geq 0$  indicates the iteration number for Newton’s method, then the solution obtained after  $n$ th step is  $\Phi^{n+1}$  as

$$\Phi^{n+1} = \Phi^n + \delta\Phi^n, \quad (50)$$

where *Newton’s update*  $\delta\Phi^n$  is given by

$$\delta\Phi^n = -(\nabla F(\Phi^n))^{-1} F(\Phi^n), \quad (51)$$

$$\nabla F(\Phi^n) \delta\Phi^n = -F(\Phi^n). \quad (52)$$

The term  $\nabla F(\Phi^n)$  denotes the *Jacobian* of  $F(\Phi^n)$ . In this work, we use (50)–(52) type of Newton's method with  $F(\cdot)$  given by

$$F(\Phi) = -\nabla \cdot \left( \frac{\nabla \Phi}{2\mu(1 + \beta\|\nabla \Phi\|^\alpha)^{1/\alpha}} \right). \quad (53)$$

The term  $\nabla F(\Phi^n)\delta\Phi^n$  is the directional gradient and can be written by using the basic definition as

$$\nabla F(\Phi^n)\delta\Phi^n := \lim_{\varepsilon \rightarrow 0} \frac{F(\Phi^n + \varepsilon \delta\Phi^n) - F(\Phi^n)}{\varepsilon} \quad (54)$$

$$= -\nabla \cdot \left( \frac{\nabla \delta\Phi^n}{2\mu(1 + \beta\|\nabla \Phi^n\|^\alpha)^{1/\alpha}} - \frac{\beta\|\Phi^n\|^{\alpha-2}(\nabla \Phi^n \cdot \nabla \delta\Phi^n)\nabla \Phi^n}{2\mu(1 + \beta\|\nabla \Phi^n\|^\alpha)^{1/\alpha+1}} \right). \quad (55)$$

The right-hand side function, which can act as a residual for the convergence of Newton's method, is given by

$$F(\Phi^n) = -\nabla \cdot \left( \frac{\nabla \Phi^n}{2\mu(1 + \beta\|\nabla \Phi^n\|^\alpha)^{1/\alpha}} \right). \quad (56)$$

Finally, the linearized version of the quasi-linear PDE (48) for Newton's update is given by

$$\begin{aligned} & -\nabla \cdot \left( \frac{\nabla \delta\Phi^n}{2\mu(1 + \beta\|\nabla \Phi^n\|^\alpha)^{1/\alpha}} - \frac{\beta\|\Phi^n\|^{\alpha-2}(\nabla \Phi^n \cdot \nabla \delta\Phi^n)\nabla \Phi^n}{2\mu(1 + \beta\|\nabla \Phi^n\|^\alpha)^{1/\alpha+1}} \right) \\ &= \nabla \cdot \left( \frac{\nabla \Phi^n}{2\mu(1 + \beta\|\nabla \Phi^n\|^\alpha)^{1/\alpha}} \right). \end{aligned} \quad (57)$$

At each *iteration step*  $n > 0$ , the goal is to compute  $\delta\Phi^n$  by using an appropriate finite-element discretization.

**Remark 4.1.** *It is known that Newton's method converges when the initial guess is sufficiently close to exact solution. Thus, for the good initial guess and when  $n = 0$ , we first solve the linear problem (choosing  $\beta = 0$  in (57)) and use it as an initial guess in the subsequent iterations. The overall error can be reduced either by using local mesh adaptivity or by choosing higher-order basis functions.*

Next, we formulate the linearized PDE (57) as a variational weak formulation on the space of test functions for finite elements. We multiply (57) by a test function  $\varphi \in W_0^{1,2}(\Lambda)$  and integrate by parts over  $\Lambda$ , then we seek  $\Phi \in W^{1,2}(\Lambda)$  that satisfies

$$\begin{aligned} & \left( \frac{\nabla \delta\Phi^n}{2\mu(1 + \beta\|\nabla \Phi^n\|^\alpha)^{1/\alpha}}, \nabla \varphi \right) - \left( \frac{\beta\|\Phi^n\|^{\alpha-2}(\nabla \Phi^n \cdot \nabla \delta\Phi^n)\nabla \Phi^n}{2\mu(1 + \beta\|\nabla \Phi^n\|^\alpha)^{1/\alpha+1}}, \nabla \varphi \right) \\ &= - \left( \frac{\nabla \Phi^n}{2\mu(1 + \beta\|\nabla \Phi^n\|^\alpha)^{1/\alpha}}, \nabla \varphi \right), \quad \forall \varphi \in W_0^{1,2}(\Lambda), \end{aligned} \quad (58)$$

where  $(\cdot, \cdot)$  is the  $L^2$  inner product.

#### 4.3. Finite-element discretization

Let  $\{\mathcal{T}_h\}_{h>0}$  be a family of elements partitioning the domain  $\Lambda$  and each  $\mathcal{T}_h$  shape regular is satisfying the minimum angle condition in the sense of Ciarlet (see [55] for details). Let  $h_K$  be the diameter of the element  $K$ , and define  $h := \max_{K \in \mathcal{T}_h} h_K$ . Each mesh in  $\mathcal{T}_h$  made of disjoint elements  $K$  is a square (or quadrilateral) in  $d = 2$ . The discretization of the domain is assumed to be approximate for the computational domain, i.e.,  $\Lambda = \bigcup_{K \in \mathcal{T}_h} K$ .

Let  $V_h$  be the space of piecewise continuous bilinear polynomials over the partition  $\mathcal{T}_h$  and is defined as

$$V_h := \{u_h \subset C^0(\bar{\Lambda}) : u_h|_K \in \mathbb{Q}^1, \forall K \in \mathcal{T}_h\} \subset H^1(\Lambda).$$

For each  $K \in \mathcal{T}_h$ ,  $\mathbb{Q}^1(K)$  denotes the bilinear polynomial on each element. Next is the discrete weak formulation of the problem: we seek  $\Phi^n \in V_h$  such that

$$a(\Phi_h, \varphi_h) = l(\varphi_h), \quad \forall \varphi_h \in V_h, \quad (59)$$

**Algorithm 1:** Algorithm for the nonlinear strain-limiting model

---

```

Input: Solution from the linear model on the coarse mesh
while [Refinement Number < Max. Number of Refinements] do
    while [Iteration Number < Max. Number of Iterations].AND.[Residual > Tol.] do
        Assemble the Jacobian (Equation (60)) and the RHS (Equation (61)) of System;
        Solve  $\delta\Phi^n$  (Equation (51));
         $\Phi^{n+1} = \Phi^n + \delta\Phi^n$  (Equation (50));
        Calculate Residual (Equation (61));
        if Residual  $\leq$  Tol. then
            | Break;
        end
    end
    Write Solution;
    Do Refinement and Transfer Solution & Interpolate onto New Mesh;
end

```

---

where  $a(\Phi_h, \varphi_h)$  and  $l(\varphi_h)$  are given by

$$a(\Phi_h, \varphi_h) = \left( \frac{\nabla \delta\Phi_h^n}{2 \mu (1 + \beta \|\nabla \Phi_h^n\|^\alpha)^{1/\alpha}}, \nabla \varphi_h \right) - \left( \frac{\beta \|\nabla \Phi_h^n\|^{\alpha-2} (\nabla \Phi_h^n \cdot \nabla \delta\Phi_h^n) \nabla \Phi_h^n}{2 \mu (1 + \beta \|\nabla \Phi_h^n\|^\alpha)^{1/\alpha+1}}, \nabla \varphi_h \right), \quad (60)$$

and

$$l(\varphi_h) = - \left( \frac{\nabla \Phi_h^n}{2 \mu (1 + \beta \|\nabla \Phi_h^n\|^\alpha)^{1/\alpha}}, \nabla \varphi_h \right). \quad (61)$$

**Remark 4.2.** From the discrete weak formulation, it is clear that the matrix corresponding to the each Newton step is symmetric and positive definite. The eigenvalues are positive and, hence, the conjugate gradient (CG) method can be used as a linear solver at each Newton step [56]. However, it is worth noting that the matrix becomes ill-conditioned when the boundary values are changed slightly and also the matrix clearly loses the positive-definite property when the gradients become larger and larger, ultimately one needs to device a special preconditioner for the CG method. For the current application, we use “symmetric successive over-relaxation” (SSOR) as a preconditioner for the CG linear solver [57].

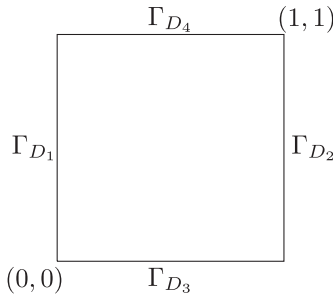
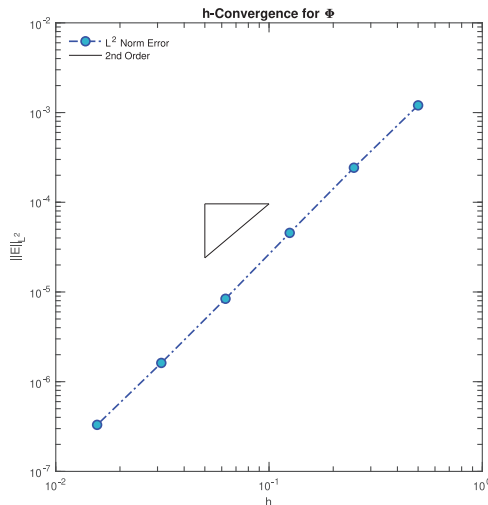
## 5. Numerical results and discussion

In this section, we explore the PDE (40) and its numerical solution that admit the “limiting” and “small” strains with unbounded, increasing near-tip stresses. We consider three different scenarios to test the efficacy and novelty of the proposed modeling framework: a classical V-notch (or wedge problem), oriented cracks, and an interface crack. A major goal in this paper is to delineate the usefulness of the nonlinear model in resolving the near-tip strains contrary to the well-known inconsistency of square-root order singular strain usually predicated by the classical linear model. It should be worth mentioning that the classical strain singularity occurs when the V-notch angle (i.e., the angle between two faces of the V-notch) is zero, but for the comparison purpose, we have considered a few non-zero wedge angles ( $10^\circ$ ,  $20^\circ$ ,  $30^\circ$ ) and performed the computations.

We would like to emphasize a fact that our numerical method is a standard bilinear continuous Galerkin finite-element method and it can best serve our immediate need. A more detailed discretization and *a priori* error estimates are topics for future study. The contemplated mathematical model is implemented using an open-source finite-element package, deal.II [58, 59], and all the numerical experiments are performed utilizing the high-performance computing (HPC) cluster at Texas A&M University-Corpus Christi. In all the numerical computations, the convergence tolerance (Tol.) for the Newton’s method is taken as  $10^{-5}$ . All the computations for this paper have been carried out on both structured and unstructured meshes. Unstructured meshes are not uncommon in the broad area of computational solid mechanics, and these are natural in dealing with complex scenarios such as crack evolution. The detailed numerical algorithm which was used in the computations for the nonlinear strain-limiting model is described in Algorithm 1.

**Table 1.** Results of the  $h$ -convergence study for  $\Phi$ .

DoFs	$L^2$ Error	Rate
25	0.00120319	—
81	0.00024265	2.7239
289	0.00004856	2.5296
1089	0.00001062	2.2917
4225	0.00000261	2.0702
16,641	0.00000065	2.0281

**Figure 1.** A domain and the Dirichlet boundary conditions for the  $h$ -convergence study.**Figure 2.**  $h$ -convergence and  $L^2$  error that shows the second-order convergence.

### 5.1. $h$ -convergence study

Before we continue to discuss the numerical implementation of the nonlinear elasticity model, we study the mesh density ( $h$ -convergence) by using a “manufactured solution.” We set a simple domain as Figure 1 and set a solution  $\Phi = \frac{\pi}{2}y^2$ . Note that this solution  $\Phi$  denotes a uniaxial tension for the domain in the  $y$ -direction. The boundary conditions are all Dirichlet and satisfy the exact solution. The numerical procedure follows Algorithm 1. For the  $h$ -convergence, we refine the whole domain globally. We have a total of 6 global refinement cycles and the number of *degrees of freedom* (DoFs) for the cycles are 25, 81, 289, 1089, 4225, and 16,641 (Table 1). Figure 2 depicts an optimal convergence order of 2, in the sense of  $L^2$ -norm, since the underlying approximation space is a bilinear polynomial. See the detailed rate values for convergence in Table 1.

### 5.2. Example 1. V-notch

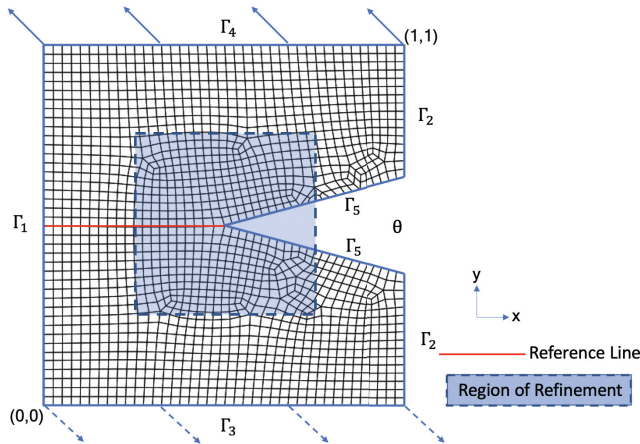
In this example, we aim to study the influence of vanishing V-notch angle on the solution and, more importantly, on the stress-strain concentration at the tip. For the notch angle ( $\theta$ ), we take four different cases: starting with

**Table 2.** Example I. Mesh refinements and number of DoFs for each case.

Refinement	Number of DoFs			
	CASE 0	CASE 1	CASE 2	CASE 3
R0	1662	1742	1792	1600
R1	3243	3416	3532	2860
R2	9450	10,010	10,282	7966
R3	33,372	35,507	36,736	27,778
R4	127,539	135,899	140,476	105,790

**Table 3.** Example I. Boundary conditions for the V-notch.

Boundary	Value
$\Gamma_1$	$\sigma_0 \times L$
$\Gamma_2$	0
$\Gamma_3$	$-\sigma_0 \times (x - L)$
$\Gamma_4$	$\sigma_0 \times (L - x)$
$\Gamma_5$	0

**Figure 3.** Example I. Two-dimensional domain for the reference V-notch (CASE 0 with R0): arrows on the boundaries denote the state of anti-plane shear. Note that the reference line is colored in red and the blue region is for local refinements.

CASE 0 with  $\theta = 30^\circ$  through  $\theta = 20^\circ$ ,  $\theta = 10^\circ$ , and  $\theta = 0^\circ$ , corresponding to CASE 1, CASE 2, and CASE 3, respectively.

The problem is formulated by taking a setting of initial coarser V-notch mesh in 2D as shown in Figure 3. The tip of the V-notch is at  $(0.5, 0.5)$ . The “blue” darker region in Figure 3 is flagged for the local mesh refinements. We successively refine the coarser mesh in this blue darker region (Algorithm 1) with four times in total. The number of DoFs for each mesh refinement is listed in Table 2, where a number next to R represents the number of the local refinements. For example, R1 is the first refinement from the original mesh (R0) in Figure 3. The “red line,” which is directly ahead of the V-notch tip at the center, serves as a reference line to compute the stresses and strains. Note that all crosses in the  $x$ -axis in the following figures such as for stress and strain line plots are indicating the distance from the left side end (or the boundary) to the other end of the reference line, i.e., the tip. The boundary conditions for the problem [30, 33] are given in Table 3, where we have  $\sigma_0 = 1.0$ ,  $L = 1.0$ . For all the V-notch problems in this example,  $\mu$  is set as 1.0 and the modeling parameter pair  $(\alpha, \beta)$  is taken as  $(0.2, 1.0)$ .

**Discussion.** First, we introduce the numerical solution obtained for the nonlinear material model. The solution  $\Phi$  to the quasi-linear PDE (40), along a reference line directly ahead of the V-notch tip, is given in Figure 4. Note that 0 for the “x” in this case is indicating the location on the left boundary ( $\Gamma_1$ ), and the green lines are for the

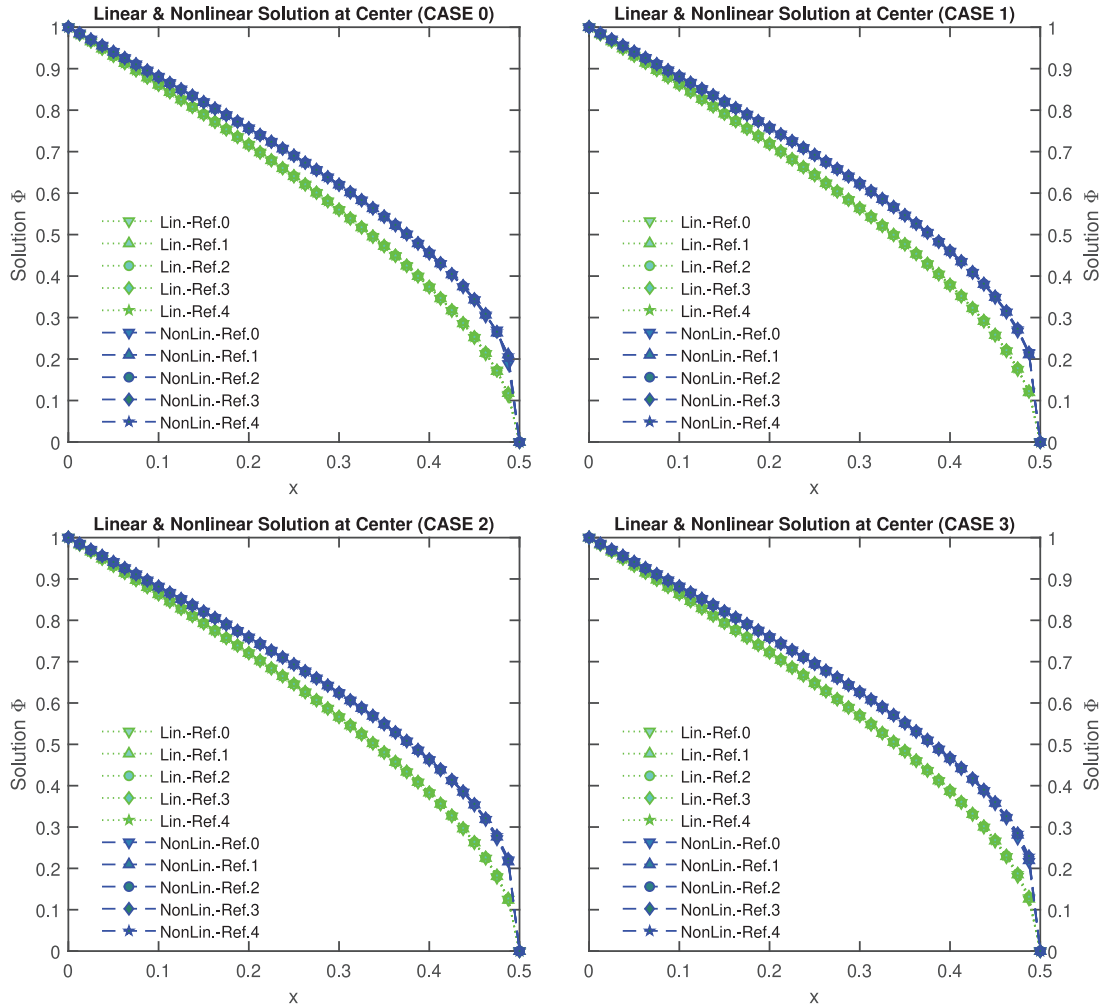


**Figure 4.** Example 1. Two-dimensional solution plot of the linear (green) and the nonlinear (blue) for cases from CASE 0 (top left) to CASE 3 (bottom right) on the reference line with every refinement.

linear model, and the blue lines are for the nonlinear, strain-limiting model. In addition, the top left of the four subfigures is the solution to CASE 0 and for each adaptively refined mesh level: from R0 to R4. Within each case, it is evidenced that there is a clear convergence of the numerical solution along the reference (red) line in the domain, where the solutions between the refinements are not distinctive but almost identical. Moreover, from these four subfigures (CASE 0 to 3) in Figure 4, the shape of the solution profile on the line remains the same among the cases of the notch angles that are decreasing.

Next, we investigate the behavior of notch-tip stress ( $\sigma_{23}$ ) and strain ( $\varepsilon_{23}$ ) of the linear and the nonlinear models on the same reference line (Figure 3). Figure 5 shows the  $\sigma_{23}$  and  $\varepsilon_{23}$  values with the semi-log scale for each case within the last refinement stage (R4). From this figure, one can clearly find a difference between linear and nonlinear material models. The difference in notch-tip strains, between linear and nonlinear models, is three orders of magnitude which suggests that the strain measure in the nonlinear problem is considerably small. These results of the nonlinear model clearly illustrate a noteworthy deviation from the classical model's *square-root order* prediction, which is specifically for the crack case (i.e., with the zero notch angle,  $0^\circ$ , i.e., CASE 3). However, there seems to be a "concentration" of notch-tip stresses in both models. However, in the nonlinear model, both stress and strain clearly behave differently near the notch tip. In other words, strains do not grow at the same rate as stresses. In Figure 6, we present contour lines for stresses and strains for CASE 3 only where both linear ((a) and (b)) and nonlinear ((c) and (d)) models are presented. We note that for the strain, the shape of contour lines for the linear model follows the same shape of the stress, while for the nonlinear model, it is clearly different from that of the stress.

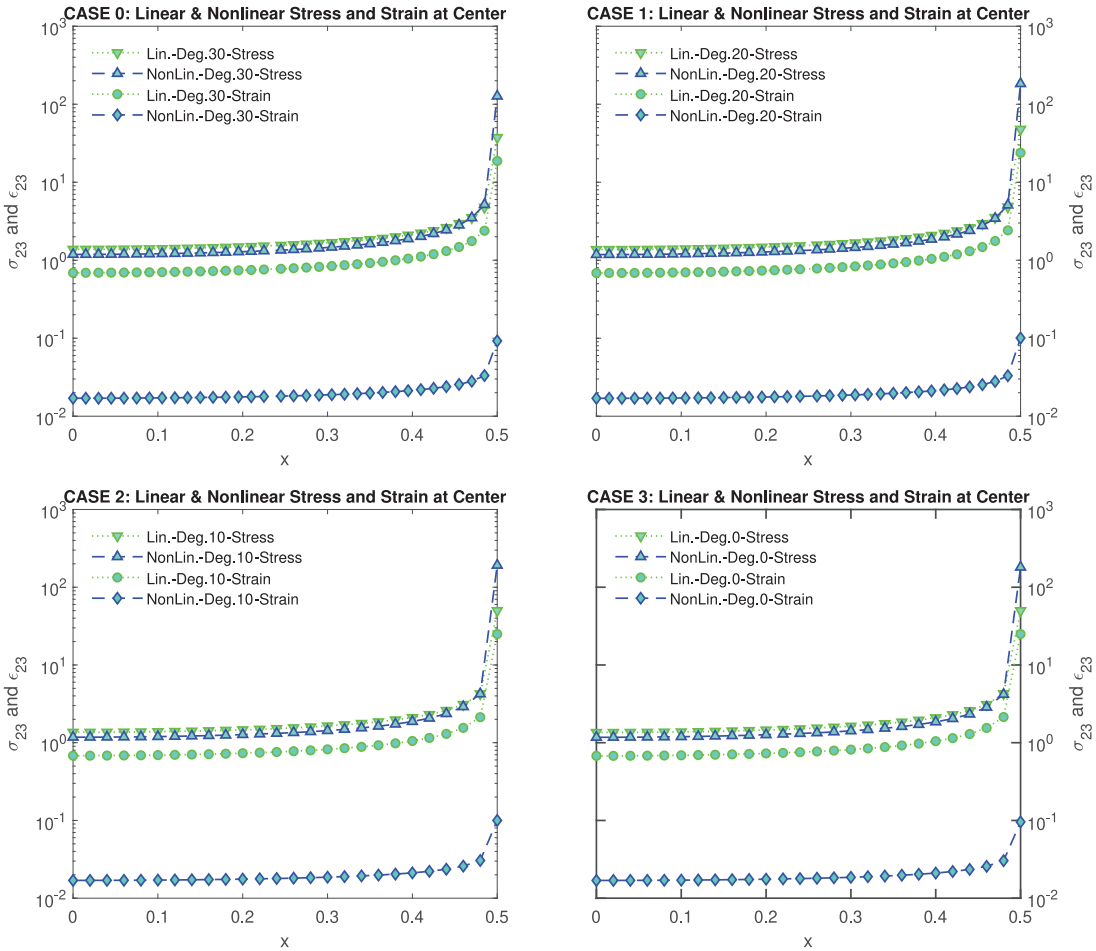


**Figure 5.** Example 1. Stress ( $\sigma_{23}$ ) and strain ( $\epsilon_{23}$ ) on the reference line expressed in semi-log scale for the linear (green) and the nonlinear strain-limiting (blue) models with the last refinement of R4: from CASE 0 (top left) to CASE 3 (bottom right).

Here, we investigate the SIF for the anti-plane strain problem. Based on Irwin's approach [60], the LEFM with polar coordinates predicts the Cauchy stress ( $\sigma_{ij}$ ) which has its origin at the tip, and it is approximated as the following formula

$$\sigma_{ij} \approx \frac{K}{\sqrt{2\pi r}} f_{ij}(\theta), \quad (62)$$

where  $f_{ij}(\theta)$  is a dimensionless quantity that depends on the load or the geometry of the structure,  $\theta$  is the polar angle, and  $K$  is the SIF. Note that the stress is proportional to  $1/\sqrt{r}$  where  $r$  is the distance from the tip. For the anti-plane strain problem, the SIF can be expressed as

$$K_{III} = \lim_{r \rightarrow 0} \sqrt{2\pi r} \sigma_{23}(r, \theta). \quad (63)$$

As for CASE 3 in Example 1, the reference line (a line that is directly ahead of the crack tip, see Figure 3) has  $\theta = 0$ , then we have

$$K_{III} := \lim_{r \rightarrow 0} \sqrt{2\pi r} \sigma_{23}(r, \theta = 0), \quad (64)$$

where  $r = 0.5$  (equivalently  $x = 0$ ) being located on  $\Gamma_1$  and  $r = 0$  (equivalently  $x = 0.5$ ) being at the tip on the reference line. For CASE 3 with R3, the linear and the strain-limiting models have the following curves for  $K_{III}$  in Figure 7. The decreasing trend in their values from the left end is due to the boundary conditions (Table 3) we impose, and it is inverted near the tip approaching the tip stresses. Note that even though the SIF formula is purely based on the solution to the linear model, it can be utilized in the nonlinear case to glean some

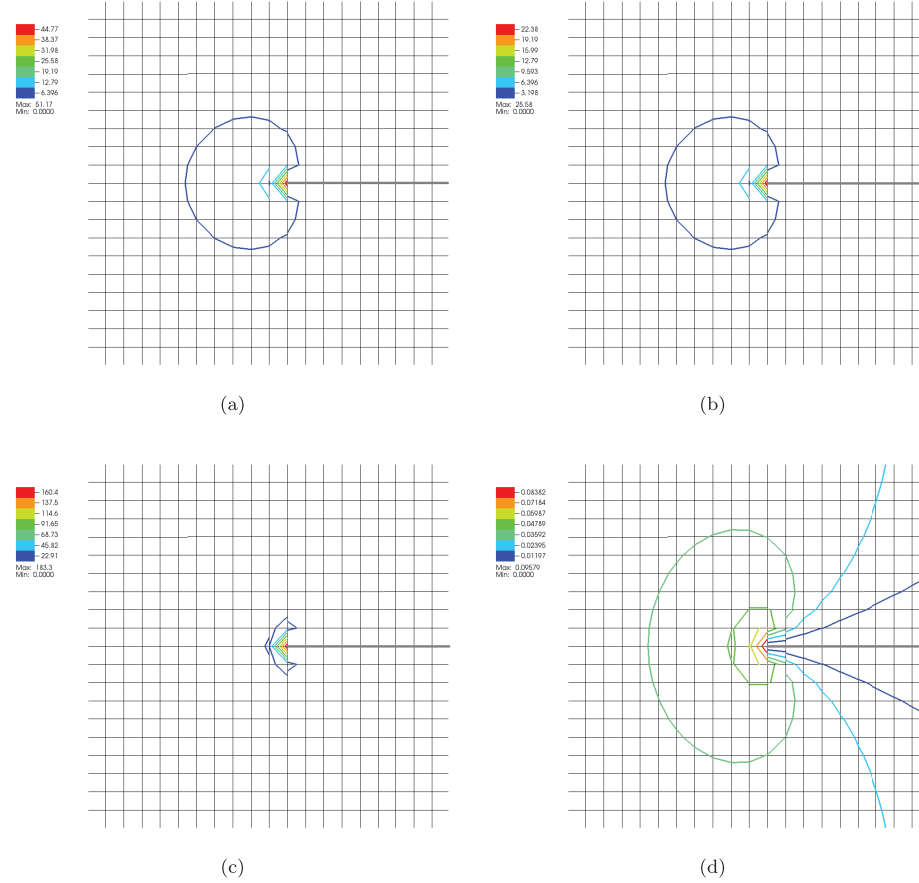


**Figure 6.** Example 1. Contour lines of  $\sigma_{23}$  and  $\varepsilon_{23}$  for CASE 3 with R4, the linear (top) versus the nonlinear (bottom): (a)  $\sigma_{23}$  for linear CASE 3; (b)  $\varepsilon_{23}$  for linear CASE 3; (c)  $\sigma_{23}$  for nonlinear CASE 3; (d)  $\varepsilon_{23}$  for nonlinear CASE 3.

important information. Furthermore, even though the strain-limiting model does not predict the same, near-tip, strain progression compared with the linear model, but definitely there is a strong evidence of singular crack-tip stress behavior. Hence, a SIF-based local fracture criterion can be used to study crack-tip evolution by using either XFEM [61] or phase-field regularization [62].

Another important question is the influence of the modeling parameter pair,  $(\alpha, \beta)$ , on the solution to the nonlinear problem as well as on the stress-strain behavior in the domain including the concentrator. A recent study [47], concerning the “limiting strain” models, has pointed out and suggested that  $\alpha$  be posed in piecewise uniform convex domains, i.e.,  $\alpha \in (0, 2)$ , for the existence of weak solutions to the boundary value problems. Here, we fix a value for  $\alpha = 1.75$ , but change  $\beta$  values as 0.01, 0.1, 1.0, 5.0, and 10.0. The results for CASE 3 with refinement of R3 are depicted in Figure 8. The influence of  $\beta$  is clearly seen in the notch-tip strains, increasing  $\beta$  results in decreasing strain values, but less considerable on stresses near the tip.

Finally, we describe the performance of our Newton’s method in each CASE and in each refinement stage. Tables 4 and 5 present the number of Newton’s iterations and corresponding residual values. We observe that Newton’s method does a commendable job in reducing the “residual” (which is the  $L^2$ -norm of  $F(\Phi)$ ) with increasing refinement overall. It is also clear from these two tables that as the notch angle decreases, the overall computation becomes expensive. Finally, Tables 6–9 are presented for CASE 0 to CASE 3, respectively, with the maximum stress and strain values along with the refinements. As indicated by the tables, larger stress and strain are obtained when the refinement (R) number is increasing, implying the trend of singular behavior. In addition, with increasing case number (CASE), i.e., as the V-notch angle is decreasing, the overall stress and strain become larger, although CASE 3 is not the largest, which might be due to the numerical interpolation with the traction-free notch boundary. We confirm that the linear model has no bounds in strain values, but the nonlinear strain-limiting is bounded around 0.1.

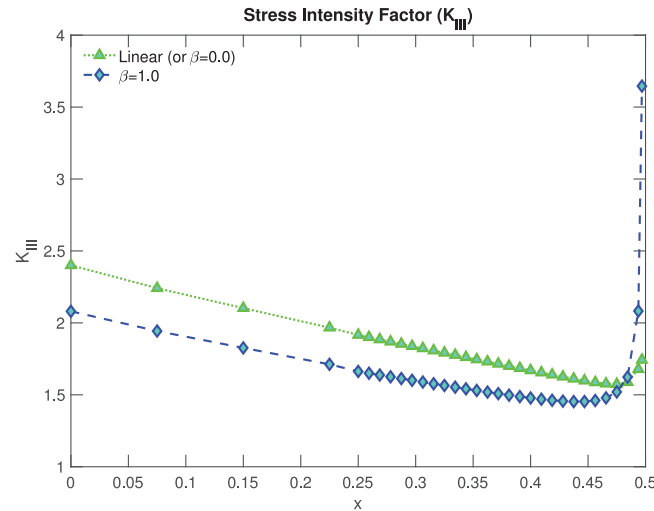


**Figure 7.** Example I. SIF for the linear (green) and the nonlinear (blue) for CASE 3 with R3.

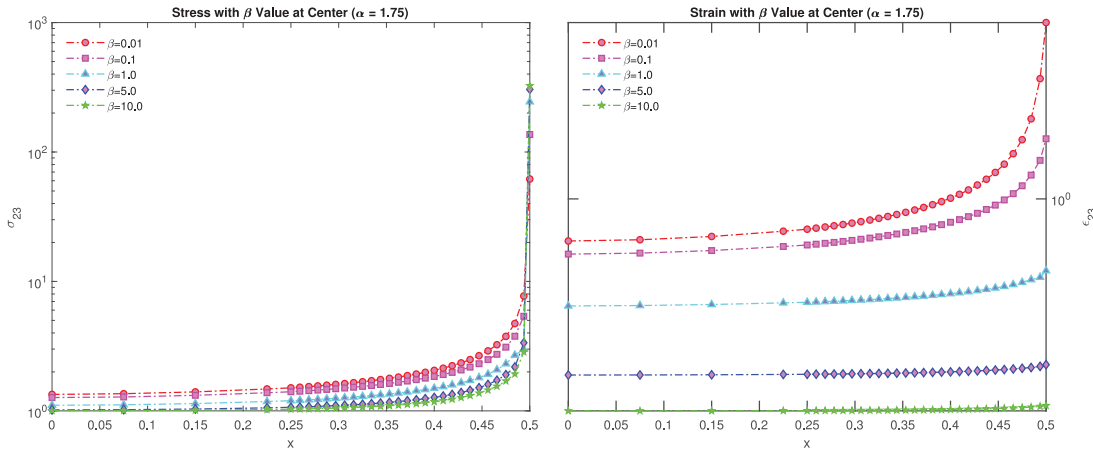


**Figure 8.** Example I. Nonlinear parameter  $\beta$  values on stress ( $\sigma_{23}$ , left) and strain ( $\varepsilon_{23}$ , right) on the reference line expressed in semi-log scale for CASE 3 with refinement of R3.

**Table 4.** Example I. Number of Newton's iterations for each case with refinements.

Ref.	Number of iterations			
	CASE 0	CASE I	CASE 2	CASE 3
R0	2	2	2	2
R1	3	3	3	10
R2	3	3	4	4
R3	3	3	3	3
R4	3	3	3	4

### 5.3. Example 2. Oriented cracks

In this example, we study the stress-strain concentration in the neighborhood of oriented cracks (not exactly symmetrical with respect to the top loading). For the computations, we take the unit square domain and crack locations as depicted in Figure 9. We have the same boundary condition as Table 3, where  $\Gamma_5$  is now for crack faces at the center of the domain. Let  $\theta$  be the angle between the “center line” of the domain (i.e.,  $y = 0.5$ ) and we set  $\theta = 0^\circ, 45^\circ$ , and  $90^\circ$ . In the post-processing, we compute the stress-strain along the “red” line leading up to the crack tip (Figure 9). The material shear modulus  $\mu$  is set as 1.0. The modeling parameter pair  $(\alpha, \beta)$  is set with two different values of  $\beta$ : 0.1 and 1.0. Thus,  $(\alpha, \beta) = (1.75, 0.1)$  and  $(1.75, 1.0)$ .

**Table 5.** Example I. Final residuals in Newton's iterations for each case with refinements.

Ref.	Final residuals ( $\times 10^{-6}$ )			
	CASE 0	CASE I	CASE 2	CASE 3
R0	1.33652	1.45545	1.60219	1.72326
R1	9.33364	7.58809	9.57336	9.63494
R2	8.62957	6.808	8.13253	9.69472
R3	6.60516	5.62745	7.82688	8.77996
R4	5.65687	7.09934	6.23879	5.62779

**Table 6.** Example I. Maximum of  $\sigma_{23}$  and  $\varepsilon_{23}$ : CASE 0.

Ref.	Linear		Nonlinear	
	$\sigma_{23}$	$\varepsilon_{23}$	$\sigma_{23}$	$\varepsilon_{23}$
R0	10.94	5.468	19.53	0.05148
R1	14.97	7.483	30.88	0.06009
R2	20.49	10.25	49.38	0.06977
R3	28.07	14.04	79.83	0.08052
R4	38.47	19.23	130.4	0.09234

**Table 7.** Example I. Maximum of  $\sigma_{23}$  and  $\varepsilon_{23}$ : CASE I.

Ref.	Linear		Nonlinear	
	$\sigma_{23}$	$\varepsilon_{23}$	$\sigma_{23}$	$\varepsilon_{23}$
R0	13.40	6.701	26.01	0.05615
R1	18.54	9.271	41.93	0.06555
R2	25.67	12.84	68.38	0.07606
R3	35.56	17.78	112.8	0.08770
R4	49.26	24.63	188.9	0.1006

**Table 8.** Example I. Maximum of  $\sigma_{23}$  and  $\varepsilon_{23}$ : CASE 2.

Ref.	Linear		Nonlinear	
	$\sigma_{23}$	$\varepsilon_{23}$	$\sigma_{23}$	$\varepsilon_{23}$
R0	13.55	6.773	25.55	0.05545
R1	18.94	9.470	41.61	0.06493
R2	26.50	13.25	68.52	0.07552
R3	37.10	18.55	114.3	0.08732
R4	51.94	25.97	192.3	0.1001

**Table 9.** Example I. Maximum of  $\sigma_{23}$  and  $\varepsilon_{23}$ : CASE 3.

Ref.	Linear		Nonlinear	
	$\sigma_{23}$	$\varepsilon_{23}$	$\sigma_{23}$	$\varepsilon_{23}$
R0	12.84	6.420	23.62	0.05260
R1	18.12	9.061	38.76	0.06175
R2	25.60	12.80	64.39	0.07204
R3	36.19	18.09	108.5	0.08352
R4	51.17	25.58	183.3	0.09579

*Discussion.* The stress and strain distributions over the domain are plotted in Figures 10, 11, and 12 for  $\theta = 0^\circ$ ,  $\theta = 45^\circ$ , and  $\theta = 90^\circ$ , respectively. From stress ( $\sigma_{23}$ ) plots, the tips are found to be under the singular stress

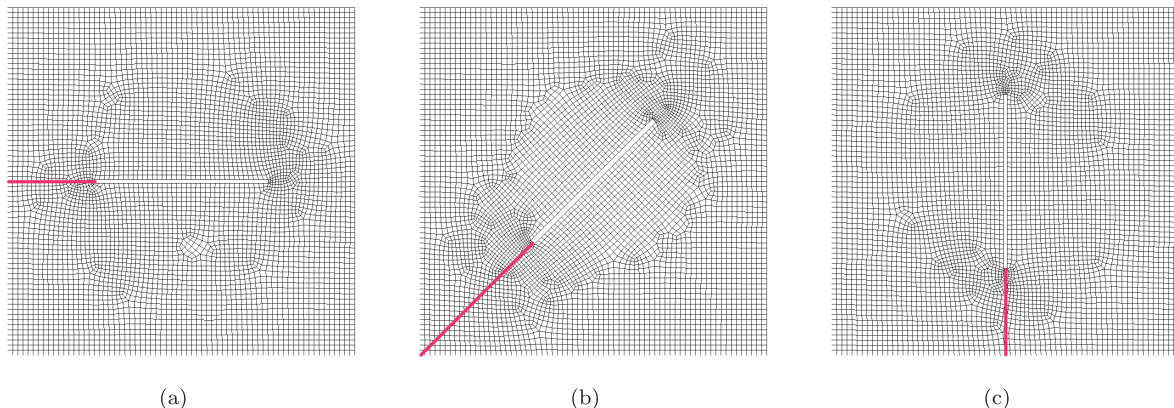


**Figure 9.** Example 2. Three cases of angle for the oriented cracks and their meshes: (a)  $\theta = 0^\circ$ ; (b)  $\theta = 45^\circ$ ; (c)  $\theta = 90^\circ$ . The reference lines are in red where stresses and strains are presented.

regardless of the angle of the crack. Thus, strains ( $\varepsilon_{23}$ ) for the linear model (or  $\beta = 0$ ) are suffering from the corresponding high values. It is clear from these figures that the strains in the nonlinear model do not grow in the same order as in the linear model for the oriented (or unsymmetrical) cracks as well. Figure 13 presents the stresses and the strains on the reference lines (Figure 9). We notice that the parameter  $\beta$  has a clear influence on stress-strain concentration, and stress increases with increasing  $\beta$  values while the strain decreases with increasing  $\beta$  values. Overall results are in consistent with the stresses and the strains on the reference lines in the previous example, except that the stress-strain curve is not presented typically but with a slight difference for the reference line for  $\theta = 90^\circ$  crack (Figure 13 (c)), where the singular maximum stress values are not right in front of the tip but near its corners.

#### 5.4. Example 3. Interface crack

In this example, we study stress-strain behavior at the tip of an interface crack. The domain  $\Omega$ , mesh, and “material interface,” which is characterized by the different values of  $\mu$ , are all depicted in Figure 14. We assume that the line  $y = 0.5, 0 \leq x < 0.5$  is a line along which two dissimilar materials are bonded together and the interface crack is lying on the line  $y = 0.5, 0.5 \leq x < 1.0$ . The two materials are perfectly bonded along the line  $y = 0.5$ . Moreover, the assumption of weak solution  $\Phi \in H^1(\Omega)$  for the variational formulation (59) is regarded as guaranteeing the continuity of displacement across the interface. The assumption of modeling the interface using two different values of  $\mu$  is similar to that made by Sigaeva and Schiavone in [63]. The boundary conditions for this problem are same as those listed in Table 3. The material body is marked by two different shear modulus for top ( $\mu_T$ ) and bottom ( $\mu_B$ ) half regions (Figure 14(a)) set with  $\mu_T = 1.8$  and  $\mu_B = 0.2$ , respectively. Being divided by the crack (the black line in Figure 14(a)), the upper region is stiffer and the average of shear modulus is 1.0 as previous problems. The modeling parameter pair in the nonlinear model,  $(\alpha, \beta)$ , is set with a single pair of  $(1.75, 1.0)$ . Our goal in this example is to study the material response under the same type of loading and then present the stress-strain computations along the reference line (the line in red in Figure 14(a)).

**Discussion.** As shown in Figure 14(b) and (d), for the linear and the nonlinear stresses, respectively, the stresses are approaching high values in the vicinity of the tip of the crack, regardless of  $\mu$  values. However, the strain patterns are different from the previous problems. The contrast in values and colors between the linear and the strain-limiting model (Figure 14(c) and (e), respectively) is attributed to the fact that the difference between the maximum strain which is located right in front of the tip and the strains for the rest in each model. For the linear model, we have similarly very small tip area especially for the bottom region (weak material) with high strain values where most areas left remain small (Figure 14(c)). For the nonlinear strain-limiting model, because the difference between the maximum strain and the rest strains decreases due to the bounded strain near the tip, the top and bottom regions are relatively in contrast (Figure 14(e)). The same results are shown in Figure 15. Owing to the line plotting of the strain on the reference line which lies sharply on the line dividing two regions

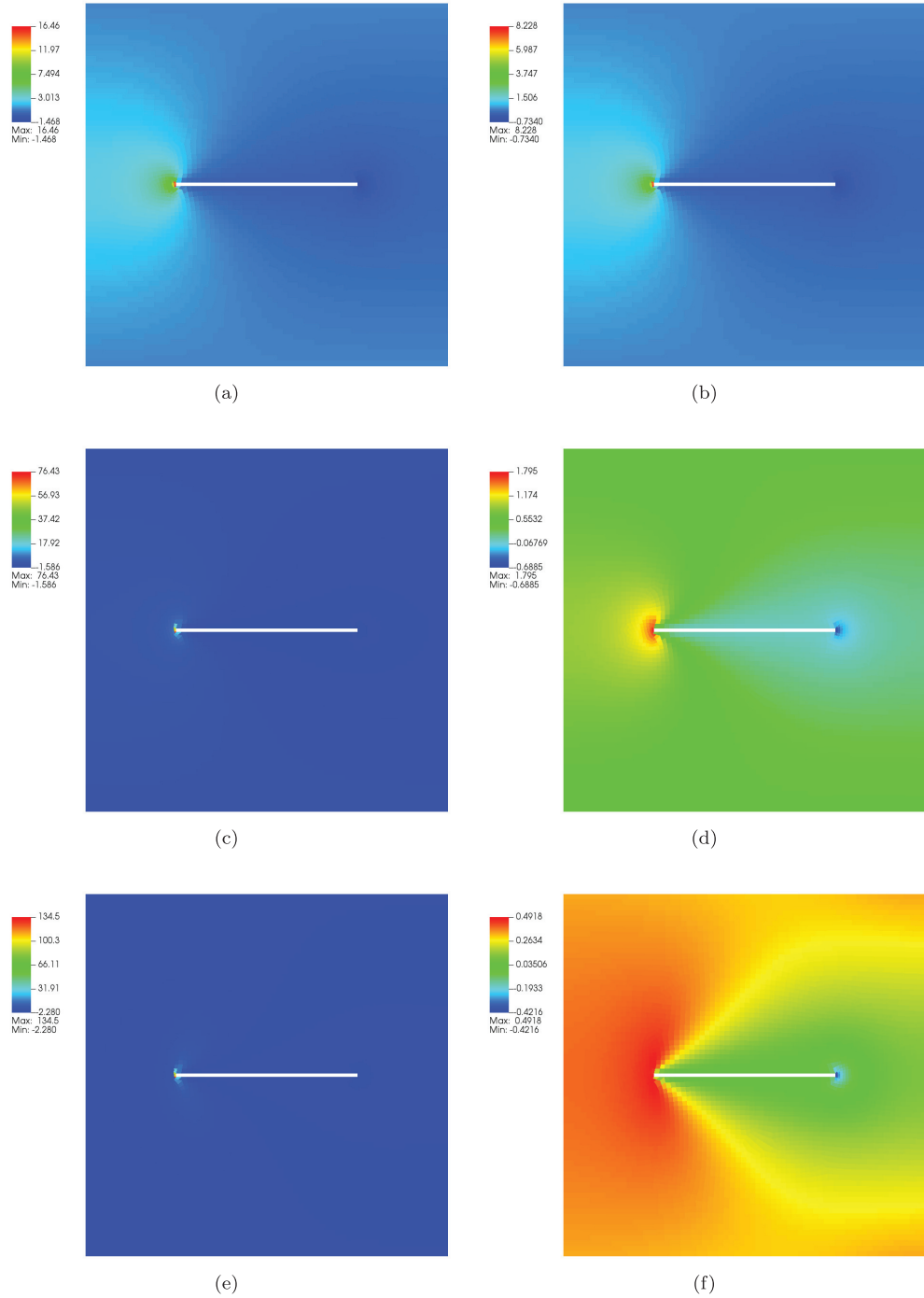


**Figure 10.** Example 2. Plots of  $\sigma_{23}$  and  $\varepsilon_{23}$  for the crack with  $\theta = 0^\circ$ : (a)  $\sigma_{23}$  for linear; (b)  $\varepsilon_{23}$  for linear; (c)  $\sigma_{23}$  for nonlinear  $\beta = 0.1$ ; (d)  $\varepsilon_{23}$  for nonlinear  $\beta = 0.1$ ; (e)  $\sigma_{23}$  for nonlinear  $\beta = 1.0$ ; (f)  $\varepsilon_{23}$  for nonlinear  $\beta = 1.0$ .

of different  $\mu$  values, the linear and the strain-limiting models are showing the averaged values between the two regions in Figure 14(a). We can see that the difference in strain values between the maximum (in the vicinity of the tip) and the minimum of the linear model are much bigger than that of the nonlinear strain-limiting model.

Finally, we investigate the same SIF analysis as Example 1 for the interface crack. Employing the same formula (64), we have the following distributions of  $K_{III}$  on the reference line (Figure 16). A slight different pattern than the SIF in Example 1 is due to the two different  $\mu$  values splitting the regions with the center line on which the SIFs are depicted.

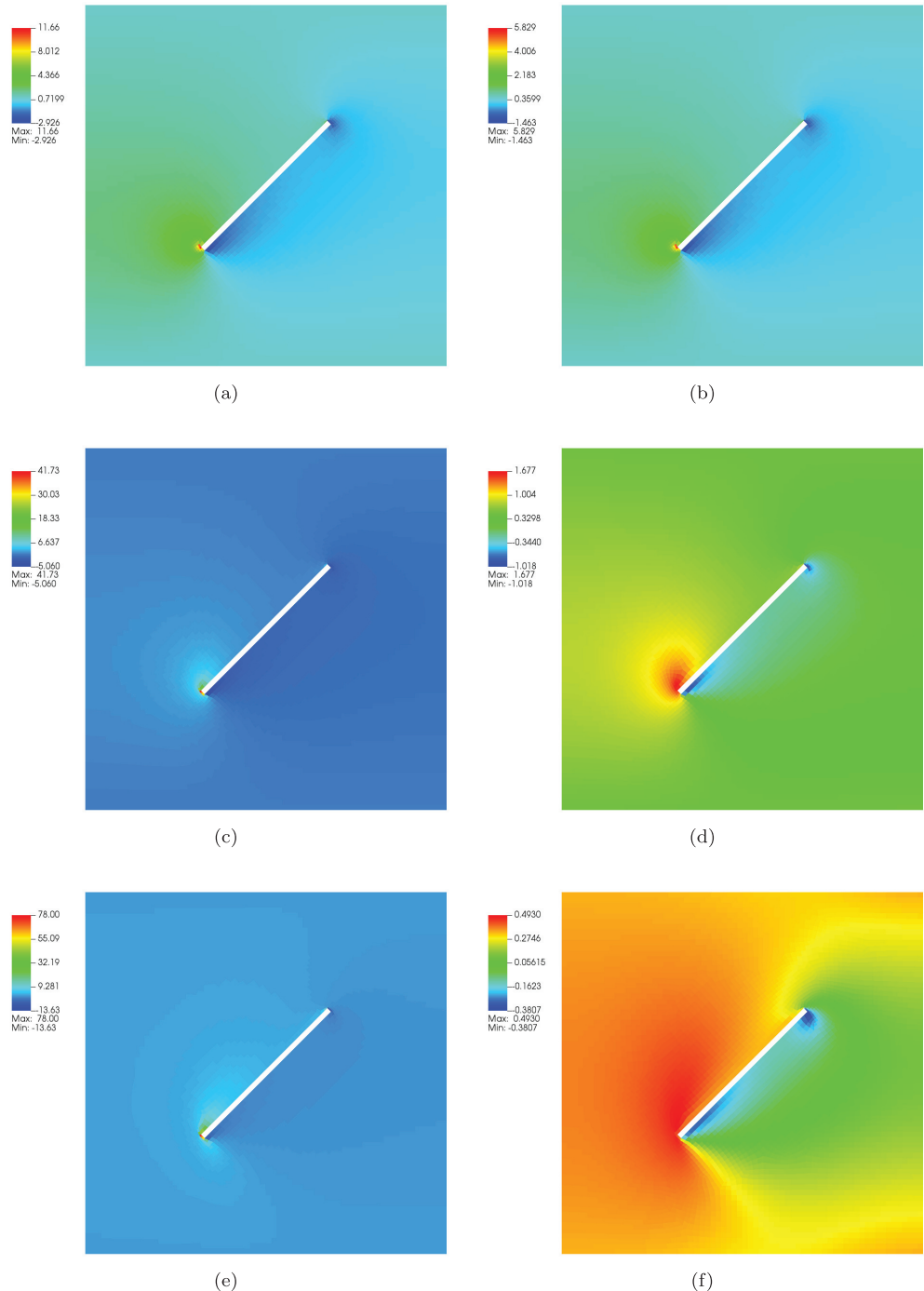


**Figure 11.** Example 2. Plots of  $\sigma_{23}$  and  $\varepsilon_{23}$  for the crack with  $\theta = 45^\circ$ : (a)  $\sigma_{23}$  for linear; (b)  $\varepsilon_{23}$  for linear; (c)  $\sigma_{23}$  for nonlinear  $\beta = 0.1$ ; (d)  $\varepsilon_{23}$  for nonlinear  $\beta = 0.1$ ; (e)  $\sigma_{23}$  for nonlinear  $\beta = 1.0$ ; (f)  $\varepsilon_{23}$  for nonlinear  $\beta = 1.0$ .

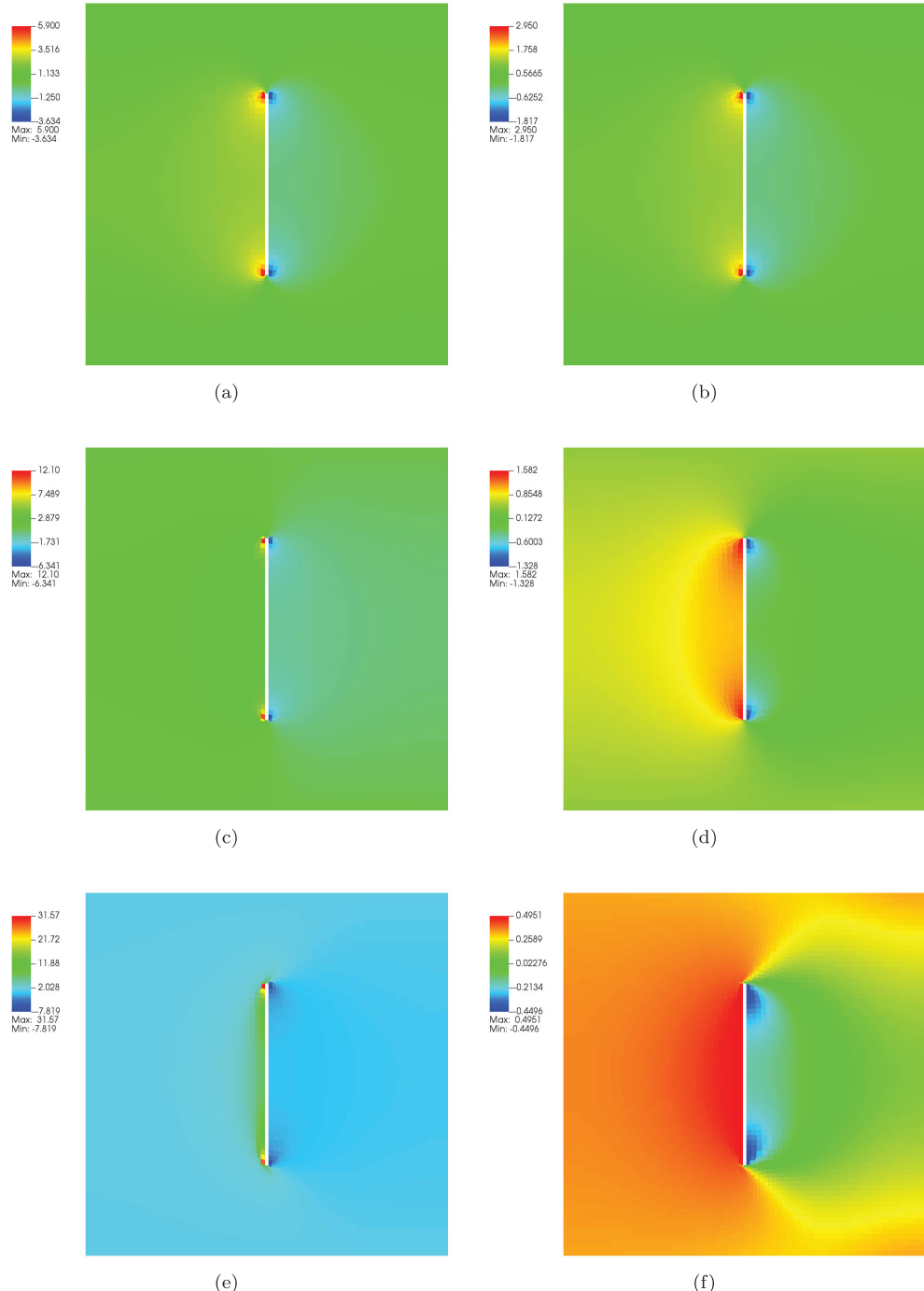


**Figure 12.** Example 2. Plots of  $\sigma_{23}$  and  $\varepsilon_{23}$  for the crack with  $\theta = 90^\circ$ : (a)  $\sigma_{23}$  for linear; (b)  $\varepsilon_{23}$  for linear; (c)  $\sigma_{23}$  for nonlinear  $\beta = 0.1$ ; (d)  $\varepsilon_{23}$  for nonlinear  $\beta = 0.1$ ; (e)  $\sigma_{23}$  for nonlinear  $\beta = 1.0$ ; (f)  $\varepsilon_{23}$  for nonlinear  $\beta = 1.0$ .

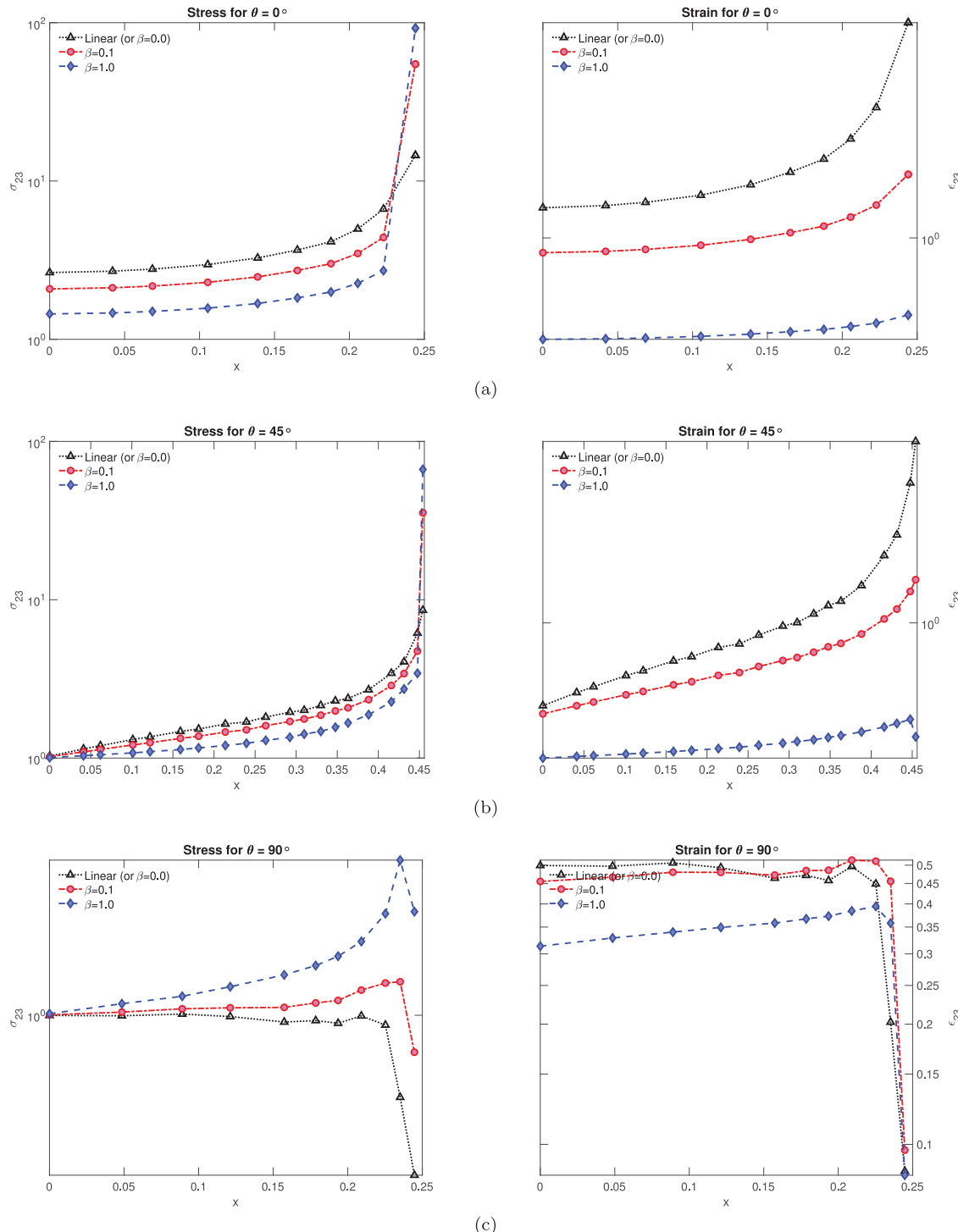


**Figure 13.** Example 2. Plots of  $\sigma_{23}$  and  $\epsilon_{23}$  on the reference lines expressed in semi-log scale: (a)  $\sigma_{23}$  (left) and  $\epsilon_{23}$  (right) for the crack with  $\theta = 0^\circ$ ; (b)  $\sigma_{23}$  (left) and  $\epsilon_{23}$  (right) for the crack with  $\theta = 45^\circ$ ; (c)  $\sigma_{23}$  (left) and  $\epsilon_{23}$  (right) for the crack with  $\theta = 90^\circ$ .

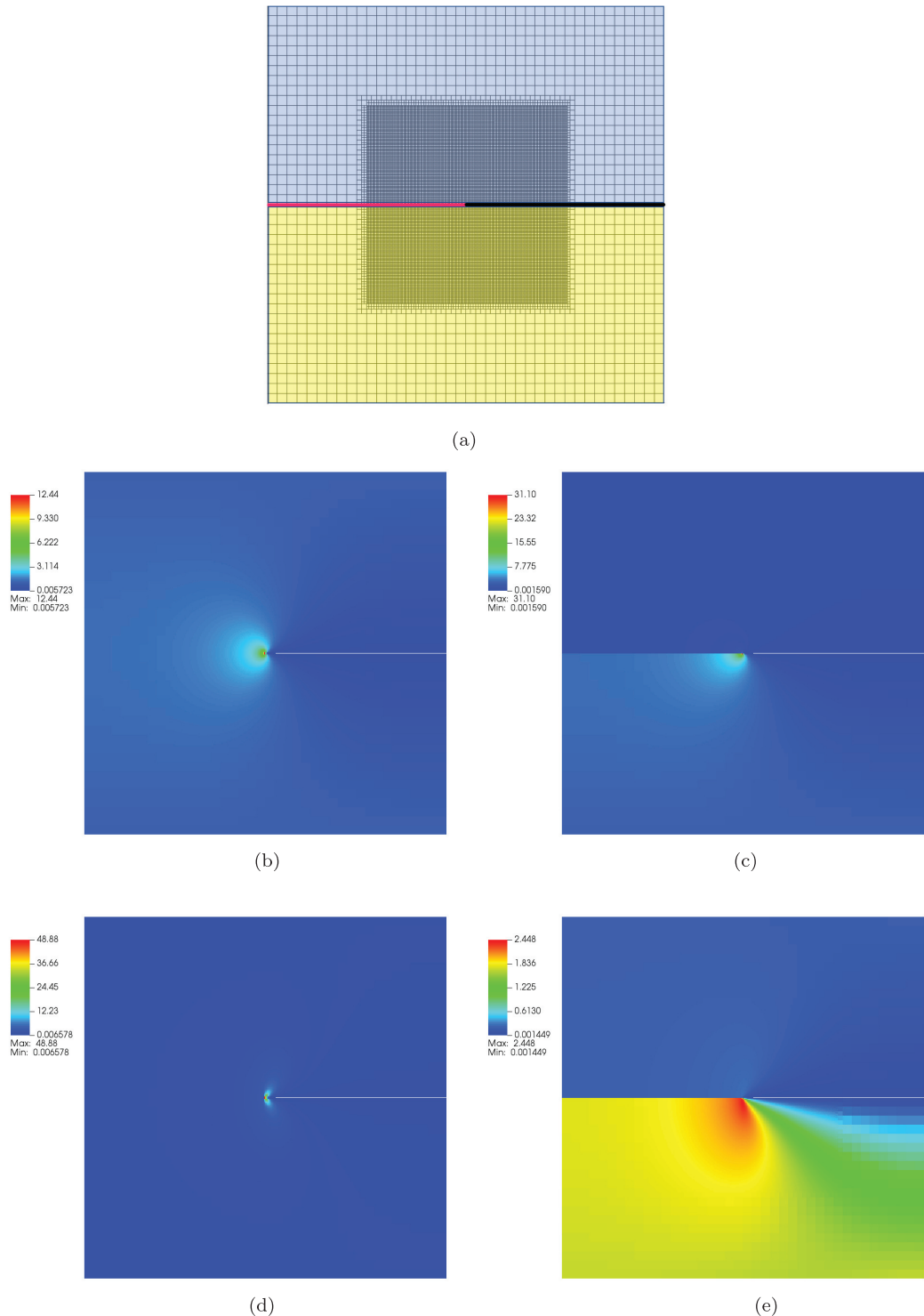


**Figure 14.** Example 3. (a) Interface crack domain and mesh: the blue region has  $\mu = 1.8$ , whereas the yellow has  $\mu = 0.2$ . (b)–(e) Plots of  $\sigma_{23}$  and  $\varepsilon_{23}$  for the interface crack: (b)  $\sigma_{23}$  for linear; (c)  $\varepsilon_{23}$  for linear; (d)  $\sigma_{23}$  for nonlinear  $\beta = 1.0$ ; (e)  $\varepsilon_{23}$  for nonlinear  $\beta = 1.0$ .

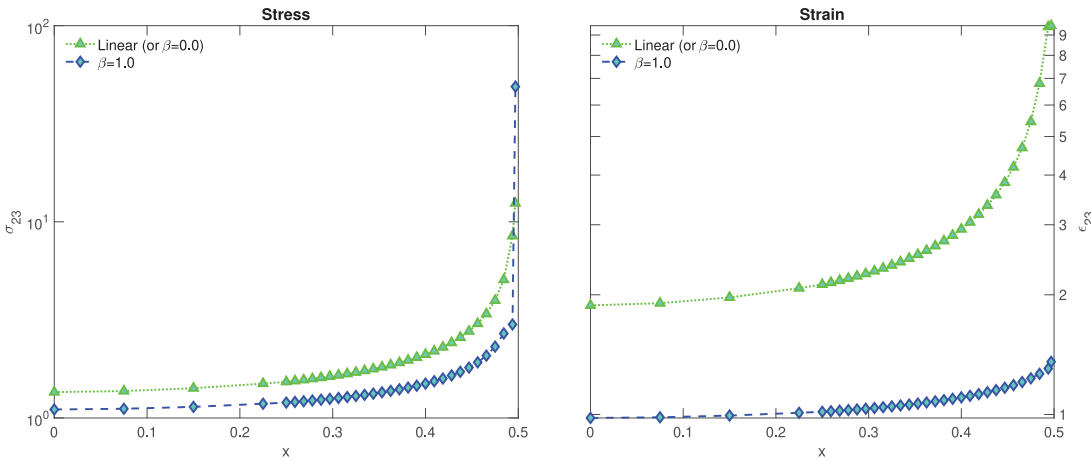


**Figure 15.** Example 3. Plots of  $\sigma_{23}$  (left) and  $\varepsilon_{23}$  (right) on the reference line expressed in semi-log scale for the linear (green) and the nonlinear strain-limiting (blue) models.

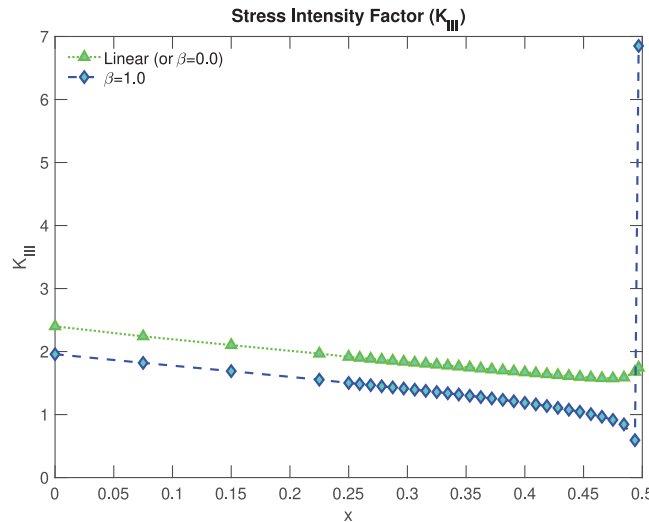


**Figure 16.** Example 3. SIF for the linear (green) and the nonlinear (blue) models.

## 6. Conclusion

In the present communication, we have studied a finite-element discretization of quasi-linear PDE arising from modeling the response of elastic solid using a framework of nonlinear strain-limiting elasticity. Our main interest was the study of the stress-strain in various problems such as V-notches, oriented cracks, and an interface crack and to characterize that the strains remain “small” whereas stresses could become high at the tips. As contemplated, the growth of near-tip strain is much slower than growth of stress. Moreover, a noteworthy result is that the existence of large stresses in the neighborhood of the crack tip in the examples of various cracks studied in this paper. More importantly, the strains predicated by the strain-limiting model are bounded and do not show the singular behavior as shown in the linear model. Another contribution of this work is the computation of SIF for the strain-limiting model using the customary formula for the LEFM and with the aid of finite-element solution obtained for the nonlinear model. Interestingly, the SIF behavior in the nonlinear model is similar to that of the LEFM. This implies that one can use the LEFM’s local fracture criterion to study the evolution of cracks within the framework of nonlinear strain-limiting of constitutive relations deliberated on in this article.

## Acknowledgments

The authors would like to thank the anonymous reviewers for their careful reading of our manuscript and their insightful comments and suggestions. The authors would like to thank the College of Science and Engineering, Texas A&M University-Corpus Christi for support.

## Funding

HCY was supported in part by the basic research fund of Korea Institute of Geoscience and Mineral Resources (KIGAM; project number GP2020-006).

## ORCID iD

S. M. Mallikarjunaiah  <https://orcid.org/0000-0002-7072-1175>

## Notes

1. By *elastic body* we mean a structure or material that is incapable of dissipating any energy.

## References

- [1] Inglis, CE. Stresses in a plate due to the presence of cracks and sharp corners. *Trans R Inst Naval Architect* 1913; 60: 219–241.
- [2] Lin, KY, and Tong, P. Singular finite elements for the fracture analysis of V-notched plate. *Int J Numer Meth Eng* 1980; 15(9): 1343–1354.
- [3] Love, AEH. *A treatise on the mathematical theory of elasticity*. Cambridge university press, 2013.
- [4] Murakami, Y, and Keer, LM. In: Murakami, Y (ed.) *Stress Intensity Factors Handbook*, Vol. 3. Kyoto: Japan, 1993.
- [5] Gurtin, ME, and Murdoch, AI. A continuum theory of elastic material surfaces. *Arch Rat Mech Anal* 1975; 57(4): 291–323.
- [6] Sendova, T, and Walton, JR. A new approach to the modeling and analysis of fracture through extension of continuum mechanics to the nanoscale. *Math Mech Solids* 2010; 15(3): 368–413.
- [7] Mallikarjunaiah, SM. *On Two Theories for Brittle Fracture: Modeling and Direct Numerical Simulations*. PhD Thesis, Texas A&M University, 2015.
- [8] Ferguson, LA, Muddamallappa, M, and Walton, JR. Numerical simulation of mode-III fracture incorporating interfacial mechanics. *Int J Fracture* 2015; 192(1): 47–56.
- [9] Zemlyanova, AY, and Walton, JR. Modeling of a curvilinear planar crack with a curvature-dependent surface tension. *SIAM J Appl Math* 2012; 72(5): 1474–1492.
- [10] Walton, JR, and Muddamallappa, M. Plane strain fracture with surface mechanics: Non-local boundary regularization. In: *Proceedings of the 24th International Congresses on Theoretical and Applied Mechanics (ICTAM)*, 21–26 August 2016, Montreal, Canada.
- [11] Broberg, KB. *Cracks and Fracture*. New York: Academic Press, 1999.
- [12] Knowles, JK, and Sternberg, E. Large deformations near a tip of an interface-crack between two neo-Hookean sheets. *J Elasticity* 1983; 13(3): 257–293.
- [13] Tarantino, AM. Nonlinear fracture mechanics for an elastic bell material. *Q J Mech Appl Math* 1997; 50(3): 435–456.
- [14] Rajagopal, KR. On implicit constitutive theories. *Applicat Math* 2003; 48(4): 279–319.
- [15] Rajagopal, KR. The elasticity of elasticity. *Z Angew Math Phys* 2007; 58(2): 309–317.
- [16] Rajagopal, KR, and Srinivasa, AR. On the response of non-dissipative solids. *Proc R Soc Lond A Math Phys Eng Sci* 463: 357–367.
- [17] Rajagopal, KR, and Srinivasa, AR. On a class of non-dissipative materials that are not hyperelastic. *Proc R Soc Lond A Math Phys Eng Sci* 465: 493–500.
- [18] Rajagopal, KR. Non-linear elastic bodies exhibiting limiting small strain. *Math Mech Solids* 2011; 16(1): 122–139.
- [19] Rajagopal, KR. Conspectus of concepts of elasticity. *Math Mech Solids* 2011; 16(5): 536–562.
- [20] Rajagopal, KR. On the nonlinear elastic response of bodies in the small strain range. *Acta Mechanica* 2014; 225(6): 1545–1553.
- [21] Rajagopal, KR, and Saccomandi, G. A novel approach to the description of constitutive relations. *Front Mater* 2016; 3: 36.
- [22] Rajagopal, KR. A note on the linearization of the constitutive relations of non-linear elastic bodies. *Mech Res Commun* 2018; 93: 132–137.
- [23] Bustamante, R, and Rajagopal, KR. A note on plane strain and plane stress problems for a new class of elastic bodies. *Math Mech Solids* 2010; 15(2): 229–238.
- [24] Bustamante, R, and Rajagopal, KR. A note on some new classes of constitutive relations for elastic bodies. *IMA J Appl Math* 2015; 80(5): 1287–1299.
- [25] Bustamante, R, and Rajagopal, KR. A nonlinear model for describing the mechanical behaviour of rock. *Acta Mechanica* 2018; 229(1): 251–272.

- [26] Bustamante, R, and Rajagopal, KR. A review of implicit constitutive theories to describe the response of elastic bodies. In: *Constitutive Modelling of Solid Continua*, pp. 187–230. New York: Springer, 2020.
- [27] Rajagopal, KR, and Walton, JR. Modeling fracture in the context of a strain-limiting theory of elasticity: A single anti-plane shear crack. *Int J Fracture* 2011; 169(1): 39–48.
- [28] Gou, K, Mallikarjunaiah, SM, Rajagopal, KR, and Walton, JR. Modeling fracture in the context of a strain-limiting theory of elasticity: A single plane-strain crack. *Int J Eng Sci* 2015; 88: 73–82.
- [29] Mallikarjunaiah, SM, and Walton, JR. On the direct numerical simulation of plane-strain fracture in a class of strain-limiting anisotropic elastic bodies. *Int J Fracture* 2015; 192(2): 217–232.
- [30] Kulvait, V, Málek, J, and Rajagopal, KR. Anti-plane stress state of a plate with a V-notch for a new class of elastic solids. *Int J Fracture* 2013; 179(1-2): 59–73.
- [31] Bulíček, M, Málek, J, Rajagopal, KR, and Walton, JR. Existence of solutions for the anti-plane stress for a new class of “strain-limiting” elastic bodies. *Calc Variat Partial Differ Eqns* 2015; 54(2): 2115–2147.
- [32] Rajagopal, KR, and Zappalorto, M. Bodies described by non-monotonic strain–stress constitutive equations containing a crack subject to anti-plane shear stress. *Int J Mech Sci* 2018; 149: 494–499.
- [33] Kulvait, V, Málek, J, and Rajagopal, KR. The state of stress and strain adjacent to notches in a new class of nonlinear elastic bodies. *J Elasticity* 2019; 135(1–2): 375–397.
- [34] Ortiz, A, Bustamante, R, and Rajagopal, KR. A numerical study of a plate with a hole for a new class of elastic bodies. *Acta Mechanica* 2012; 223(9): 1971–1981.
- [35] Ortiz-Bernardin, A, Bustamante, R, and Rajagopal, KR. A numerical study of elastic bodies that are described by constitutive equations that exhibit limited strains. *Int J Solids Struct* 2014; 51(3–4): 875–885.
- [36] Bridges, C, and Rajagopal, KR. Implicit constitutive models with a thermodynamic basis: a study of stress concentration. *Z angew Math Phys* 2015; 66(1): 191–208.
- [37] Kambapalli, M, Kannan, K, and Rajagopal, KR. Circumferential stress waves in a non-linear cylindrical annulus in a new class of elastic materials. *Q J Mech Appl Math* 2014; 67(2): 193–203.
- [38] Kannan, K, Rajagopal, KR, and Saccomandi, G. Unsteady motions of a new class of elastic solids. *Wave Motion* 2014; 51(5): 833–843.
- [39] Bustamante, R, and Sfyris, D. Direct determination of stresses from the stress equations of motion and wave propagation for a new class of elastic bodies. *Math Mech Solids* 2015; 20(1): 80–91.
- [40] Magan, AB, Mason, DP, and Harley, C. Two-dimensional nonlinear stress and displacement waves for a new class of constitutive equations. *Wave Motion* 2018; 77: 156–185.
- [41] Magan, AB, Mason, DP, and Harley, C. Elastic waves in a circular cylinder and cylindrical annulus for a subclass of implicit constitutive equations. *Math Mech Solids* 2020; 25(2): 201–233.
- [42] Erbay, HA, and Şengül, Y. Traveling waves in one-dimensional non-linear models of strain-limiting viscoelasticity. *Int J Non-Lin Mech* 2015; 77: 61–68.
- [43] Itoui, H, Kovtunenko, VA, and Rajagopal, KR. On the states of stress and strain adjacent to a crack in a strain-limiting viscoelastic body. *Math Mech Solids* 2018; 23(3): 433–444.
- [44] Zhu, H, Muliana, A, and Rajagopal, KR. On the nonlinear viscoelastic deformations of composites with prestressed inclusions. *Composite Struct* 2016; 149: 279–291.
- [45] Şengül, Y. Viscoelasticity with limiting strain. *Discrete Contin Dynam Syst* 2021; 14(1): 57–70.
- [46] Bulíček, M, Málek, J, Rajagopal, KR, and Süli, E. On elastic solids with limiting small strain: modeling and analysis. *EMS Surv Math Sci* 2014; 1(2): 293–342.
- [47] Bulíček, M, Málek, J, and Süli, E. Analysis and approximation of a strain-limiting nonlinear elastic model. *Math Mech Solids* 2015; 20(1): 92–118.
- [48] Gelmetti, N and Suli, E. Spectral approximation of a strain-limiting nonlinear elastic model. *Matematički Vesnik* 2018; 71(1-2).
- [49] Bonito, A, Girault, V, and Süli, E. Finite element approximation of a strain-limiting elastic model. *IMA J Numer Anal* 2020; 40(1): 29–86.
- [50] Truesdell, C. Hypo-elasticity. *J Rat Mech Anal* 1955; 4: 83–1020.
- [51] Mai, T, and Walton, JR. On strong ellipticity for implicit and strain-limiting theories of elasticity. *Math Mech Solids* 2015; 20(2): 121–139.
- [52] Mai, T, and Walton, JR. On monotonicity for strain-limiting theories of elasticity. *J Elasticity* 2015; 120(1): 39–65.
- [53] Bustamante, R. Some topics on a new class of elastic bodies. *Proc R Soc A Math Phys Eng Sci* 2009; 465(2105): 1377–1392.
- [54] Bulíček, M, Málek, J, Rajagopal, KR, et al. Existence of solutions for the anti-plane stress for a new class of “strain-limiting” elastic bodies. *Calc Variat Partial Differ Eqns* 2015; 54(2): 2115–2147.
- [55] Ciarlet, PG. *The Finite Element Method for Elliptic Problems*. Philadelphia, PA: SIAM, 2002.
- [56] Saad, Y. *Iterative Methods for Sparse Linear Systems*. Philadelphia, PA: SIAM, 2003.
- [57] Eisenstat, SC. Efficient implementation of a class of preconditioned conjugate gradient methods. *SIAM J Sci Statist Comput* 1981; 2(1): 1–4.
- [58] Alzetta, G, Arndt, D, Bangerth, W, et al. The deal. II library, version 9.0. *J Numer Math* 2018; 26(4): 173–183.
- [59] Bangerth, W, Heister, T, and Kanschat, G. *deal.II Differential Equations Analysis Library, Technical Reference*, 2013. Available at: <http://www.dealii.org> (accessed 15 May 2021).

- [60] Irwin, G. Analysis of stresses and strains near the end of a crack traversing a plate. *J Appl Mech* 1957; 24: 361–364.
- [61] Belytschko, T, and Black, T. Elastic crack growth in finite elements with minimal remeshing. *Int J Numer Meth Eng* 1999; 45(5): 601–620.
- [62] Bourdin, B, Francfort, GA, and Marigo, JJ. Numerical experiments in revisited brittle fracture. *J Mech Phys Solids* 2000; 48(4): 797–826.
- [63] Sigaeva, T, and Schiavone, P. The effect of surface stress on an interface crack in linearly elastic materials. *Math Mech Solids* 2016; 21(6): 649–656.